Chapter 4

Remote Mapping of Sea Surface Currents Using HF Doppler Radar Networks

Chapter Outline

Real-time sea surface current measurements are needed for applications such as port operations, surveys, and oil-slick dissipation. Operational oceanography has not yet reached meteorology's operational level, primarily because progress in numerical modeling still has to be made and routine data assimilation is still to be developed. Until the arrival of remote sensing technologies and their routine application on a real-time basis, surveying companies and similar agencies had to rely heavily on *in situ* real-time current measurements for assisting offshore operations. Although providing valuable information, this approach is costly (human and ship costs for at-sea operations, instrument deployment, and so on), time consuming (often moorings have to be deployed for lengthy periods to gather enough data for reliable statistics to be established), and somewhat incomplete in terms of budget considerations in the sense that only scattered point measurements can be made (Vigan, 2002).

Forecasts cannot be established with *in situ* data. To predict local water circulation, even at relatively short time scales, a large area must be monitored synoptically with a high spatial and temporal coverage. Based on these considerations, and thanks to the technological leap achieved in the last few decades, the present trend in sea surface current measurements is to use remote sensing technologies.

Remote sensing in the oceanographic context is the science of making measurements from a distance without placing measuring instruments into physical contact with the sea surface. Applications of remote sensing technologies are especially valuable, and sometimes crucial, in coastal waters when the survival of conventional instrumentation becomes rather difficult because of rough weather conditions or other local factors.

The ideal tool for measurement of surface currents in coastal water bodies should be a land-based system that remotely scans the sea surface day and night at a rapid rate in all weather conditions and provides real-time vector maps of the surface current patterns at close spatial and temporal intervals. Although the backscattering mechanism underlying the radio wave Doppler radar technique for sea surface current mapping (Figure 4.1) was discovered by D. D. Crombie in the early 1950s (Crombie, 1955), nonavailability of miniature computers required for online digital signal processing hampered the development of an operational sea surface current mapping system for more than two decades after the discovery was made.

The basic mechanism underlying the application of radio wave (HF/VHF) Doppler radar systems for sea surface current mapping is that the phase velocity of sea

Measuring Ocean Currents. http://dx.doi.org/10.1016/B978-0-12-415990-7.00004-1

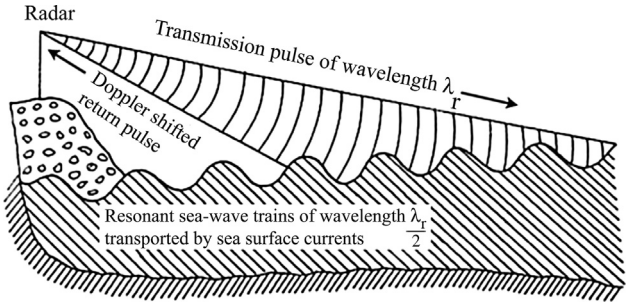

FIGURE 4.1 Schematic of the Bragg resonant backscattering of radio wave pulses from a Doppler radar impinging on the sea surface. *(Source: In part from Barrick et al., 1977.)*

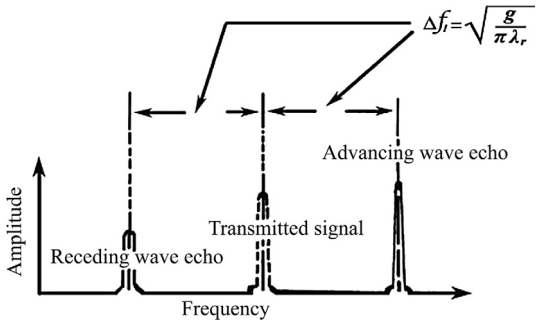

FIGURE 4.2 Schematic illustration of the Doppler shift Δf_1 of the ideal first-order backscattered sea echo spectrum of HF/VHF Doppler radar signal in the presence of sea surface gravity waves propagating on still water. λ_r is the radar wavelength. *(Source: Barrick et al., 1977.)*

surface waves is altered by the underlying water currents. The basic interaction between electromagnetic (EM) and ocean waves is *backscattering*. When EM waves transmitted from radar impinge upon a rough sea surface, a certain amount of incident energy is reflected, or *scattered*, back to the radar. This return signal contains information about the sea surface. The two basic processes or mechanisms responsible for backscatter of EM energy from the sea surface are specular reflection and Bragg scattering. If there exists some relative motion between the radar and the target (sea surface in the present case), the return signal exhibits a shift in frequency (i.e., the frequency of the received signal is different from the frequency of the transmitted signal). This shift in frequency, known as *Doppler shift*, is directly related to the relative velocity and inversely proportional to the radar wavelength. The return signal, displayed as a Doppler frequency spectrum, is analyzed to provide information on the motion of the target.

4.1. CROMBIE'S DISCOVERY

In the 1950s, while monitoring the HF radio wave signals backscattered from the sea surface, D. D. Crombie, a communications engineer, observed two peculiar and unique dominant peaks in its spectrum. The observed spectrum was unique because whereas the familiar Doppler spectrum of the radio wave echoes from a discrete target, such as an aircraft, shows only one peak, the spectrum of backscattered radar signals from the sea surface revealed the following spectacular peculiarities:

- Two well-defined peaks were present, and these were placed on either side of the radar transmission frequency, representing positive and negative Doppler peaks (Figure 4.2).
- The displacement of these peaks from the transmission frequency varied as a function of the square root of the transmission frequency rather than in direct proportion to the transmission frequency, as in the case of the Doppler echo from a discrete target.
- The strength of the positive and the negative Doppler peaks was proportional to the height of the advancing and the receding sea waves but was much larger than that expected from a discrete wave (target).

From conventional knowledge, we know that one target can generate only one echo, and therefore a "casual" observer would have attributed the second echo to the presence of "electrical noise" or "instrument noise" in the radar system. However, Crombie's "observing" mind did not allow him to neglect the observed double peaks as mere "instrument noise." Rather, he believed that he could be on the verge of a great discovery.

Based on the hitherto unreported unique peculiarities that he observed in the spectrum of the backscattered signals from the sea surface, Crombie sought to establish his discovery of the scattering mechanism as follows:

- Because the Doppler echoes consist of two discrete peaks placed on either side of the radar transmission frequency, these echoes must be originating from two targets (located on the sea surface) that move apart at a constant velocity.
- These two targets must be the advancing and the receding sea surface waves.
- The considerably enhanced strength of the two Doppler peaks compared to those of discrete targets of the same size (in the present case, sea surface waves) must be attributed to a resonant backscattering mechanism.

Based on this sound reasoning, Crombie postulated that the strong backscatter of HF radio waves emanating from the sea surface is a form of Bragg scattering, resulting from resonant sea surface wave trains lining up to form a diffraction grating for the radio waves. Conceptually, Bragg resonance can be described as the constructive reinforcement of radio waves reflected back selectively from those sea surface waves having half the incident radio wavelength, in a manner analogous to X-ray diffraction from the arrays of atoms in a crystal lattice. Although the heights of ocean waves are generally small compared to

the HF/VHF radar wavelength, the backscattered echo is surprisingly large and readily interpretable in terms of its Doppler features.

Based on the arguments Crombie put forward, he postulated that, in the absence of sea surface currents, the sea-echo spectrum consists, to first order, of two sharp lines with positive and negative Doppler shifts. These Doppler shifts correspond to the phase velocity of radially advancing and receding sea surface waves (i.e., those waves of which the wavefronts are oriented in the direction of the radar) of one-half the radar wavelength. A steady sea surface current transports the sea surface waves so that their apparent phase velocity, as measured by a stationary observer, is the sum of their phase velocity in still water (i.e., nonmoving water) and the component of near-surface current in the direction of wave travel. Any shift in the measured phase velocity of the sea surface wave from its theoretical still-water value in deep water can, therefore, be related directly to the vector component of the sea surface current moving toward or away from the radar site.

It may be noted that phase velocity of deep-water waves is considered here for convenience, because of its mathematical simplicity relative to that of shallow-water waves. HF/VHF radar can therefore infer radial surface current from the amount of displacement of the "Bragg lines" of the echo spectrum from symmetry about zero Doppler (see Figure 4.3). The HF/VHF part of the electromagnetic spectrum is important because one-half the incident radio wavelength, corresponding to the HF/VHF frequencies, is comparable to the wavelengths of typical sea surface gravity waves.

In principle, Crombie's hypothesis provided a means for estimation of radial components of water currents at different cells on the sea surface. Measurements of range-Doppler spectra from different cells on the sea surface using two widely separated radars would thus enable mapping of two-dimensional sea surface current vectors at every individual cell.

The theory behind the application of the Doppler radar principle for remote measurement of sea surface currents is as follows: In the absence of underlying water current, sea

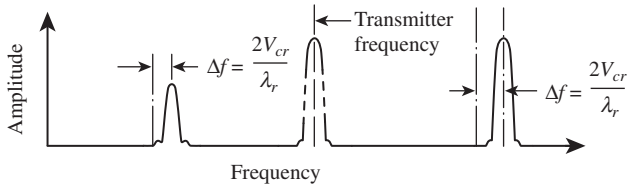

FIGURE 4.3 Schematic illustration of the displacement Δf of the first-order backscattered sea-echo spectrum of HF/VHF Doppler radar signal in the presence of sea surface gravity waves propagating over an underlying radial current V_{cr}. Note that λ_r is the radar wavelength. *(Source: Barrick et al., 1977.)*

surface wave trains of a given wavelength L propagate in deep water with a phase velocity U_o given by

$$U_o = \sqrt{\frac{g}{k}}, \tag{4.1}$$

where $k = \frac{2\pi}{L}$ and g is the acceleration due to gravity. Thus, from Equation 4.1,

$$U_o = \sqrt{\frac{gL}{2\pi}} \tag{4.2}$$

Assuming that the radar "sees" the sea surface gravity wave as a "target," the velocity V_1 of the sea surface gravity wave trains in the direction of the radar can be calculated from the well-known Doppler shift Δf_1 for target speed, namely:

$$\Delta f_1 = \frac{2V_1}{\lambda_r} \tag{4.3}$$

where λ_r is the radar wavelength. Alternatively, substituting the relation $c = f\lambda_r$ in Equation 4.3, we get

$$\Delta f_1 = \frac{2fV_1}{c}, \tag{4.4}$$

where f and c are the frequency and propagation speed, respectively, of the radar transmission signal.

From Equation 4.3,

$$V_1 = \lambda_r \frac{\Delta f_1}{2}. \tag{4.5}$$

Equating the "target" velocity to the phase velocity of deep-water gravity waves in the absence of an underlying water current, we get

$$\lambda_r \frac{\Delta f_1}{2} = \sqrt{\frac{gL}{2\pi}}, \tag{4.6}$$

where L is the wavelength of the sea surface gravity wave. According to Crombie's hypothesis, Bragg resonance occurs when $L = \frac{\lambda_r}{2}$. By substitution of $L = \frac{\lambda_r}{2}$ in Equation 4.6, we get

$$\Delta f_1 = \sqrt{\frac{g}{\pi\lambda_r}}. \tag{4.7}$$

This frequency depends only on the radar transmission wavelength and is termed the *Bragg frequency*.

Substituting $\frac{c}{f}$ for λ_r in Equation 4.7, we get

$$\Delta f_1 = \sqrt{\frac{gf}{\pi c}}, \tag{4.8}$$

This explains the observed square-root relationship between the Doppler shift and the radar transmission frequency. Any Fourier decomposition of a random but

finite patch of sea surface gravity waves always contains wave spectral energy at or near the required wavelength and direction to satisfy the Bragg resonance condition. Thus, discrete resonant Doppler peaks are always observed in the spectrum of the backscattered echoes from the sea under all sea states (except totally calm sea).

The presence of underlying water current displaces the Doppler spectra unidirectionally from their symmetrical positions, relative to the radar transmission frequency (Figure 4.3). It is from this displacement that an estimate of the radial current component is made, making the assumption that sea surface gravity waves and the underlying surface currents are linearly superimposed. The first-order scattering mechanism is highly selective in terms of the direction of wave propagation; that is, only those resonant sea surface gravity waves that are traveling radially toward or away from the radar contribute appreciable energy to the first-order echo. A second-order spectrum is also generated, but this is of no interest in the remote measurement of sea surface current.

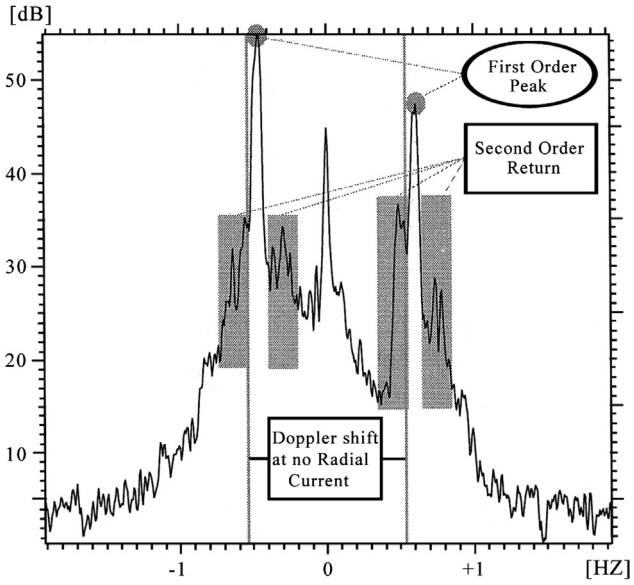

FIGURE 4.4 Measured HF Doppler spectrum of the backscattered radio-wave signal from the sea surface. First-order lines and second-order side bands are indicated. *(Source: Gurgel et al., 1999.)*

4.2. PECULIARITIES OF PULSE DOPPLER-RADAR ECHO SPECTRA

An examination of the Doppler frequency spectrum of the return echo shows two distinct regimes. The first-order regime, or echo, is characterized by a sharp and distinct peak at a frequency corresponding to the sea surface wave satisfying the Bragg resonant condition. The second-order regime is the continuum portion of the spectrum and contains more information on the sea surface properties. This portion is caused by scatter from all sea surface waves and provides, after analysis, the directional wave-height spectrum. Thus, because of the presence of "first-order" and "higher-order" components, the observed Doppler spectra of the backscattered sea echo are more complicated than the ideal situation depicted in Figures 4.2 and 4.3.

A real situation is illustrated in Figure 4.4. The dominant spectral features explained by the simple, lowest-order terms of the perturbation analysis (Barrick, 1972) are referred to as a *first-order* sea echo, and the remaining less dominant features are termed *higher-order* because they arise from the smaller (i.e., second-order, third-order, etc.) terms. The large first-order resonant peaks are usually more dominant than the higher-order peaks but are insensitive to the sea state. The first-order lines are usually very sharp, often only a few millihertz wide. The second-order features, which result from wave-wave interactions, are highly sensitive to the sea state and manifest themselves as sidebands of the first-order echo (Weber and Barrick, 1977). This results in a natural broadening of the first-order peaks. However, the presence of the second-order side bands does not alter the position of the first-order Bragg lines. As long as its position can be accurately determined, the second-order continuum does not affect the current measurement capability of the Doppler radar system.

For all practical purposes, the backscattered sea echo-signal amplitude is a Gaussian random variable. This applies to both the first- and the second-order portions of the echo. The echo is random because of the statistical nature of the scattering sea surface. Furthermore, the sea surface current flow field immediately beneath the waves is not laminar but turbulent. This also contributes to the randomness of the received backscattered echo. The observed spectra are, therefore, often complicated in structure and of peculiar definitions, depending on the nature of the sea surface, currents, and the shallowness of the water body. Accordingly, the observed spectra can be categorized into different types (Eccles, 1989), such as:

- Classical (i.e., two narrow Bragg lines)
- Typical (two Bragg lines with a higher-order continuum surrounding them)
- Split lines (two close sets of Bragg lines)
- Turbulence (broad spiky Bragg lines)
- Shallow water (definite Bragg lines at less than normal Bragg separation)
- Stormy sea (large second-order component)
- Complex (several large peaks and confusing features)

In regions of strong spatial gradients in the surface circulation, two sets of Bragg lines are frequently observed, indicating the presence of two current regions. In such cases, to derive a representative radial current value, the two current values are weighted according to the signal

strength of the Bragg lines. In shallow waters, the phase velocity of the sea surface gravity waves decreases compared to that of the deep-water waves. This results in the Bragg lines of the Doppler spectrum to be at less than normal separation. If the sea surface is devoid of any disturbances (i.e., gravity waves are absent), the frequency of the backscattered signal received by the radar will be equal to the frequency of the transmitted signal, and consequently the Bragg resonance will be absent. The resulting spectrum is called a *single-line spectrum* because the Bragg lines are absent. Some of the complications of the received signals and various aspects of signal detection schemes have been discussed by Leise (1984). Shay et al. (1995) have observed that even in a clearly wave-laden sea, normally only one Bragg peak is available in the spectra of the return signal originating from extreme ranges (i.e., close to the theoretical limit of the radar range). Measurements by Skop et al. (1995) indicated that propagation across land (during current measurements from bays and estuaries) decreases the signal strength, as expected, but does not result in extraneous Doppler peaks. The reduction in power at the Doppler peaks can be related to the amount of land mass swept by the signal. Certain anomalous behavior in the Doppler spectra appears in shoal regions during periods of low tide. The anomalous returns and the complexities in very shallow-water spectra are yet to be fully understood.

4.3. ESTIMATION OF SEA SURFACE CURRENT USING THE BRAGG RESONANCE PRINCIPLE

The mathematical expression for sea surface current measurements using Doppler radar systems is derived as follows: It is assumed that sea surface waves are accompanied by an underlying water current, at least the Stokes' drift generated by the waves. Let the sea surface wave ride on current with a radial velocity V_2. The Doppler radar recognizes this wave as a target, which moves with a velocity V_2. The Doppler shift Δf_2 detected by the radar is given by the Doppler equation:

$$\Delta f_2 = \frac{2fV_2}{c} \tag{4.9}$$

Current-driven displacement of the observed Bragg resonance peak from the expected still-water Bragg resonance peak is given by

$$\Delta f = \Delta f_2 - \Delta f_1 \tag{4.10}$$

From Equations 4.8–4.10,

$$V_2 = \left(\frac{c}{2f}\right)\left[\Delta f + \left(\sqrt{\frac{gf}{\pi c}}\right)\right] \tag{4.11}$$

However, V_2 is the vector sum of the radial velocity of the surface current V_{cr} and the phase velocity U_o of the resonant sea surface gravity waves propagating toward and away from the radar in still water. Thus,

$$V_{cr} + U_o = V_2 \tag{4.12}$$

However, for $k = \frac{2\pi}{L}$ (from wave theory) and $L = \frac{\lambda_r}{2}$ (Bragg resonance condition), the phase velocity of the resonant gravity waves can be expressed as:

$$U_o = \sqrt{\frac{gL}{2\pi}} = \sqrt{\frac{g\lambda_r}{4\pi}} = \sqrt{\frac{gc}{4\pi f}} \tag{4.13}$$

From Equations 4.11–4.13, we get:

$$V_{cr} = \frac{c\Delta f}{2f} \tag{4.14}$$

Thus, the displacement Δf by the Doppler peak of the radar echoes (see Figure 4.3), resulting from a radial current V_{cr}, is given by the expression:

$$\Delta f = \frac{2fV_{cr}}{c} = \frac{2V_{cr}}{\lambda_r} \tag{4.15}$$

Thus,

$$V_{cr} = \frac{\Delta f \lambda_r}{2} \tag{4.16}$$

The radar transmission frequency f is usually in MHz and the displacement Δf is usually in Hz. Therefore, for convenience, if f is expressed in MHz and the displacement Δf is expressed in Hz, the radial surface current V_{cr} (in m/s) can be denoted by the expression

$$V_{cr} = 150\left(\frac{\Delta f}{f}\right) \tag{4.17}$$

4.4. DEPTH EXTENT OF DOPPLER RADAR-BASED SEA SURFACE CURRENT MEASUREMENTS

The depth extent of sea surface current measurements using the HF/VHF Doppler radar-based Bragg resonance principle is not related to the penetration depth of the incident electromagnetic radiation. The penetration depth δ of the incident electromagnetic wave is given by the expression

$$\delta = \sqrt{\frac{2}{\omega\mu\sigma}} \tag{4.18}$$

where ω is the angular frequency (radian/s) of the radar transmission wave, μ is the permeability of the medium ($\mu = 4\pi \times 10^{-7}$), and σ is the conductivity ($\sigma = 4.3$ Siemens/m). Based on the above considerations,

the penetration depth of the incident electromagnetic radiation of ~27 MHz is approximately 4.7 cm.

The depth-extent of Doppler radar-based sea surface current measurements is a complicated function of the depth extent of those sea surface waves that are responsible for Bragg scattering. Thus, the radar-derived sea surface current measurements represent a depth-integrated value in the uppermost water column. The phase velocity U of a sea surface wave superimposed on an underlying water current is a function of the wave number k of the sea surface wave, the vertical current profile $V(z)$ over depth z, and $\exp(-2kz)$ as given by the expression:

$$U = U_o \pm 2k \int_0^\infty V(z) \exp(-2kz) dz \tag{4.19}$$

where U_o is the phase velocity of the sea surface wave in still water. Thus, the unidirectional displacement Δf of the Bragg spectra is the result of a depth-averaged current, with $\exp(-2kz)$ as a weighting function. However, the vertical current profile $V(z)$ is sheared and depends on various factors such as the hydrodynamic characteristics of the locality, wind characteristics, and so forth. Accordingly, the vertical current may have (1) an exponential profile, (2) a linear profile, or (3) a logarithmic profile. The effective radar sampling depth thus depends on the near-surface water-current structure. The sampling depths for linear, exponential, and logarithmic profiles are given by $\left(\frac{\lambda_r}{8\pi}\right)$, $0.7\left(\frac{\lambda_r}{8\pi}\right)$, and $0.011\lambda_r$, respectively (Collar, 1993). The sampling depth is typically 2–3 m, which is extremely close to the sea surface compared with other more familiar current measurements. The dependence of the mean sampling depth on the wavelength of the incident electromagnetic wave (i.e., radar wavelength, λ_r) can provide a means of investigating the vertical structure of water current very close to the sea surface if multifrequency transmissions are made. Because longer sea surface waves are affected by deeper currents than are shorter sea surface waves, the water-current shear close to the ocean surface can be estimated by varying the radar transmission frequency.

4.5. TECHNOLOGICAL ASPECTS OF DOPPLER RADAR-BASED SURFACE CURRENT MAPPING

Vertically polarized electromagnetic signals are used in the HF/VHF Doppler radar technology of sea surface current measurement because seawater is an excellent electric conductor at these frequencies. Thus, in addition to the radar wavelength, the radar polarization is another important specification of the system. *Polarization* is the orientation (i.e., direction) of the electric vector in the electromagnetic radiation related to the terrain. A sketch of a vertically polarized electromagnetic wave is shown in Figure 4.5. All electromagnetic waves propagate along straight lines in free space and, therefore, cannot generally propagate to other surface points below the horizon. However, in *ground-wave* mode, the vertically polarized propagating fields at these frequencies follow the curvature of the Earth and continue well into the shadow region beyond the horizon, even in the absence of atmospheric and ionospheric refractive-index anomalies (Barrick, 1972; Barrick et al., 1974; Barrick et al., 1977). Thus, using the ground-wave mode of propagation (Ponsford and Srivastava, 1990), targets can be detected at a range far greater than conventional sky-wave microwave radar. It may be noted that horizontally polarized propagating fields are never used in ground-wave propagation because a horizontally polarized sea echo is quite sensitive to the incidence angle (Barrick et al., 1974). High-frequency (HF) over-the-horizon (OTH) radars have been used for mapping sea surface currents over very large ocean areas. In this case, although the measurements are not affected by clouds or precipitation, they are subject to ionospheric distortion. In the case of OTH radars, ionospheric motions shift the sea-echo spectrum in the same way that currents do, thereby making it difficult to separate the two effects. One method to reduce the effects of ionospheric motions in OTH radars is to employ the nearby land echo as a zero-Doppler reference (Maresca and Carlson, 1980). Another possibility is to use the less stable ionospheric reflections by averaging the measurements taken at different times (i.e., low-pass filtering), taking advantage of the shorter

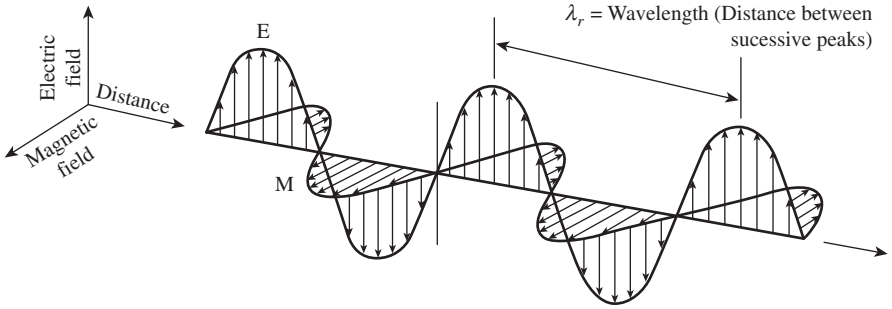

FIGURE 4.5 Sketch of a vertically polarized electromagnetic wave.

time variability of the ionosphere compared with that of ocean currents (Georges and Harlan, 1995).

It may be noted that the overall displacement of the entire Doppler spectrum, as a result of the transport of the sea surface waves by the underlying water current, is considerably smaller compared to the Doppler shift in the spectrum solely due to the phase velocity of the sea surface waves. Nevertheless, this small overall displacement is measurable. The Doppler spectra illustrated in Figures 4.2 and 4.3 are idealized representations. The observed spectra are often buried in noise. Discrimination of the signal from noise is a problem of digital signal processing. Online signal processing and estimation of sea surface currents are accomplished by special-purpose algorithms using microcomputers or minicomputers, which form an integral part of the electronic hardware of the Doppler radar system.

4.6. EXPERIMENTAL DEVELOPMENTS

Crombie employed vertically polarized HF radio waves propagating at grazing incidence to make practical use of his concept for remote mapping of sea surface currents using Doppler radar (Crombie, 1972). In his experiments, the backscattered echoes from the sea surface were measured from two known narrow azimuthal sectors on the sea surface. As with all pulse-Doppler radar systems, time gating of the received echo signal referenced to the transmitted pulse determines the range to the measurement location (i.e., the radar footprint, or illuminated sea surface area, from where the sea-echo originated). The footprint size is determined by range and radar beam width, which is a function of antenna size. For a real-aperture radar system, radar beam width and aperture are related by the expression:

$$\phi = 1.2\left(\frac{\lambda_r}{D}\right) \tag{4.20}$$

where ϕ and D are the radar beam width and the antenna aperture, respectively. Thus, the narrow beam width required for fine spatial resolution can be achieved only with a large antenna.

At any given instant in time, the backscattered signals are received from an angular section of the sea surface located at a given distance (say, R) from the antenna, given by the following equation:

$$R = \frac{ct}{2} \tag{4.21}$$

where c is the velocity of the radar transmission signal (i.e., 3×10^8 m/s) and t is the elapsed time between pulse transmission and return. The radial width β of the annulus (Figure 4.6) depends on the transmitted pulse width τ given by the expression:

$$\beta = \frac{c\tau}{2} \tag{4.22}$$

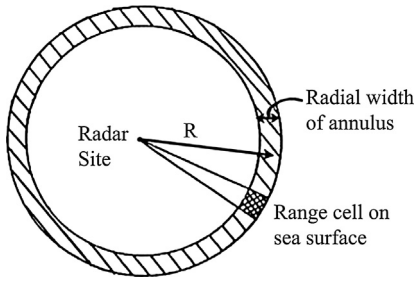

FIGURE 4.6 Backscatter from a range cell on a circular annulus of radius R.

whereas the angular width (of the range cells) corresponds to the receiving-antenna beam width. Thus, for pulse-Doppler radar, the radial range resolution is determined by the width of the transmitted radar pulse. For example, if the transmission pulse width τ is 20 μs, the signal sample from each range (time) gate would represent the echo from an annulus of the sea surface 3 km in width, concentric with the radar location. A noteworthy feature in this arrangement is that the system processes data from all azimuths in the same spectral analysis integration time. For a total distance of 75 km from the radar, time-gated echoes from a total of 25 consecutive concentric cells $\left(\text{i.e.,}\frac{75}{3}\right)$ are received and digitized. A pulse-Doppler radar system typically produces several velocity values in a given radar cell, which is a segment of a range cell defined by the azimuth angle from the radar and azimuth increment (see illustration in Lipa et al., 2006). These values are averaged to obtain the final output value for that location, and the standard deviation is calculated (Lipa et al., 2006). It is evident that their standard deviation increases with range as more vectors are included in the larger radar cells.

HF radar systems use different methods of spatial resolution in both range and azimuth. Range resolution is conventionally achieved by means of short pulses. Azimuthal resolution is achieved by means of direction finding (phase comparison) and beam forming. In both cases it is assumed that the transmit antenna is omnidirectional or slightly directed toward the sea, and azimuthal resolution is performed by means of an array of receive antennas. Each single antenna receives echoes from different azimuthal directions, which are superimposed.

Historically, sea surface current-mapping, direction-finding (DF) antennas and algorithms have taken several forms. Barrick et al. (1977) and Gurgel (1997) used antenna elements separated by short distances and relied on phase-path differences to extract bearing, which is an ingenious technique originally conceived by Crombie. The direction-finding method is based on the Fourier decomposition of the time series received by three or four antennas. Each Fourier line is attributed to a Doppler shift and in turn to a radial speed. It is assumed that the different radial speeds

arrive from different directions, which are determined by comparing the amplitudes and phases at the receive antennas. Figure 4.7 illustrates the principle of direction finding for a single plane wave, i.e., one Fourier component. To avoid ambiguities, the diagonal of the antenna array must be equal to or less than $\frac{\lambda_r}{2}$. Some further information on direction-finding algorithms is presented by Gurgel and Essen (1998) and Gurgel et al. (1999).

In the DF technique, the phase difference between the echo signals received at any two of the receiving antenna elements is used to obtain the angular direction of arrival of the echoes with reference to the line joining the receiving antenna elements. This is shown in Figure 4.8. The phase difference (ϕ degrees) of the plane wave front received at the two antenna elements is related to the corresponding path difference l. Because a phase difference of 360° corresponds to a path difference of λ_r, the measured phase

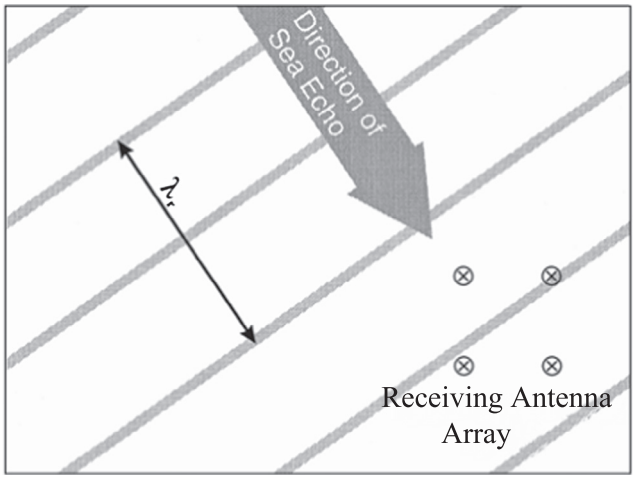

FIGURE 4.7 Principle of direction finding for a single plane wave, i.e., one Fourier component. The diagonal of the square antenna array is equal to or less than $\frac{\lambda_r}{2}$. *(Source: Gurgel et al., 1999.)*

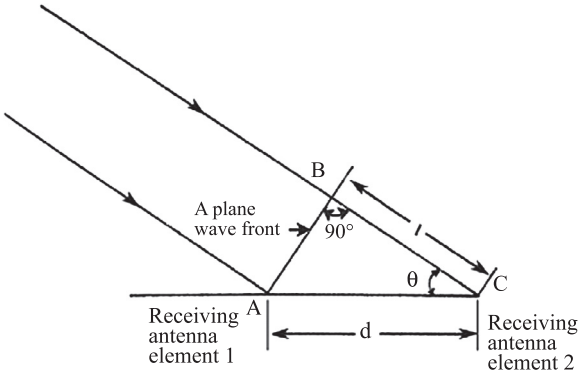

FIGURE 4.8 Diagram showing the principle of estimation of the direction of arrival (θ) of an echo with reference to the line joining the receiving antennas. l is the path difference of a plane wave front at the two receiving antenna elements, and d is the separation between the receiving antenna elements.

difference (ϕ degrees) corresponds to a path difference l, given by the expression:

$$l = \frac{\lambda_r \phi}{360} \tag{4.23}$$

where l is expressed in the same unit as λ_r. Referring to Figure 4.8,

$$l = d(\cos\theta) \tag{4.24}$$

From Equations 4.23 and 4.24, we get

$$\theta = \cos^{-1}\left(\frac{\lambda_r \phi}{360d}\right) \tag{4.25}$$

Because λ_r and d are known for a given arrangement of the receiving antenna elements and ϕ is measured, the direction of arrival θ of the echo with reference to the receiving antenna elements can be estimated. Thus, by comparing the phases between two noninteracting antennas separated by a known distance (usually less than $\lambda_r/2$), it is possible to uniquely determine the direction of arrival of the signal over a sector of 180° or less. In the experimental stages, Barrick et al. (1977) employed three collinear independent receiving antennas, each separated by distance $\lambda_r/4$ and aligned parallel to a straight coastline. The three-element system was later changed to a four-antenna configuration (arranged in a square) to resolve two signals from 360°. This permitted the operation of the radar on peninsula or island. A detailed description of the four-element receiving antenna system is given by Jeans and Donnelly (1986).

The main advantage of direction finding is the small extend of the receive antennas array (i.e., $\lambda_r/2$). The direction-finding method of achieving azimuthal resolution has been applied successfully for surface current measurements. The main disadvantage of the direction-finding method is that it is not appropriate for extracting information on the sea state. This is because the second-order signal (which contains the sea surface wave information) from a certain direction is masked by first-order signals from deviating directions (Gurgel et al., 1999). Another disadvantage is the assumption that the different radial velocities all come from different directions, which might be invalid in a very inhomogeneous current field. Subdividing the time series in overlapping parts and using sophisticated algorithms help overcome this limitation. However, the beamforming method of achieving azimuthal resolution does not depend on such an assumption.

An alternative way to gain directional information on currents, and additionally on waves, is to form a set of real narrow beams. As mentioned earlier, large antenna arrays are needed to do this (see Figure 4.9), and they can be both expensive and cause siting problems. The output of a linear array of several receiving antennas (typically, 16) can be combined, in a process known as *beam forming*, to make narrow beams that are generally limited to a minimum

FIGURE 4.9 An example of installation of a linear array of HF Doppler radar receive antenna close to the seacoast. *(Source: Hammond et al., 1987.)*

width of about λ_r/D radians, where λ_r is the radar wavelength and D the overall length of the array. The optimum distance of adjacent antenna elements of the array is $\lambda_r/2$.

The advantage of beam forming is that the beam can be steered to achieve particular area coverage. Beam forming generally increases the antenna gain, which in turn increases the signal-to-noise ratio of the echoes received. Modern digital beam formers can also be configured to form nulls in the antenna pattern in the direction of any interfering radio systems.

The oldest types of beam formers make use of time delays in cables. If all the cables from the antennas to the receiver are of the same length, then a beam is formed along the boresight perpendicular to the array. By introducing a progressive increase in cable length from one end of the array to the other, the beam can be steered to either side of the boresight as required, up to a practical maximum of perhaps 45°. The just mentioned time-delay beam formers are slow and unreliable but have the great advantage of having a very wide instantaneous bandwidth.

The effect of a time delay at each antenna can be reproduced by electronically inserting the equivalent phase change. It is much quicker to steer a beam using such phase beam steering. Furthermore, the unreliability, expense, and weight of cables and switches can be avoided. There are many ways of electronically changing the phase of a radio signal, and the only real disadvantage of these systems, the limited instantaneous bandwidth, is not usually a problem for HF radar sea sensing (Gurgel et al., 1999).

The most advanced type of forming antenna patterns is digital beam forming. In this scheme, each antenna element in the array has its own receiver and analog-to-digital converter, and the beams are formed by digitally processing all the outputs. The system is very flexible, and beams can be recalculated to any shape and even formed after the experiment. Different weighting (window) functions can be applied to control the antenna side lobes, and correction factors can be built in to account for the end elements of the array behaving in a different way from those at the center. The WERA radar of Gurgel et al. (1999) uses this type of beam forming, as shown in Figure 4.10. A typical idealized beam formed from a 16-element array parallel to the coast is shown in Figure 4.11.

A practical difficulty affecting most long linear arrays is the problem of erecting them on a straight coastline (see Figure 4.9). When two radar systems are used to map the sea surface currents from an area of water, the two arrays must be installed at an angle to the coast; otherwise their beams will not intersect (which is a necessary criterion to generate surface current vector maps of the region under consideration). When the two arrays are installed at an angle to the coast, antenna elements at one end of the array must necessarily be erected closer to the sea than those at the other. The differential radio propagation along land/sea paths is so great that the beams formed have much larger side lobes than

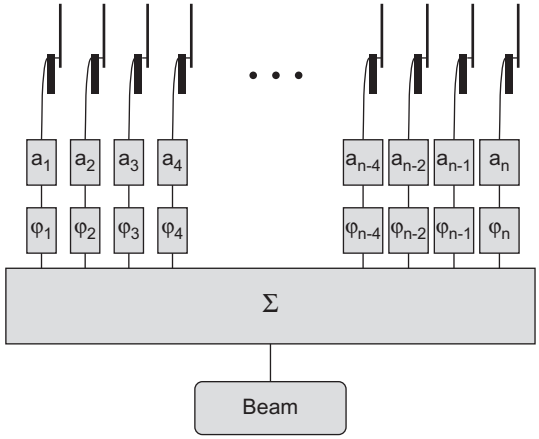

FIGURE 4.10 Principle of beam forming. After weighing by a_i and phase shifting by φ_i, the signals of n receive antenna signals are added. *(Source: Gurgel et al., 1999.)*

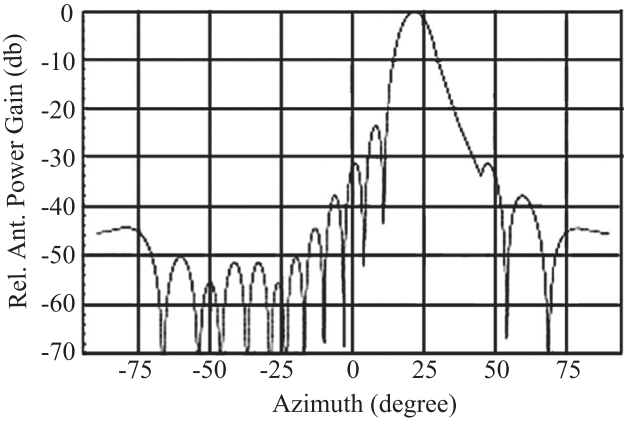

FIGURE 4.11 The theoretical antenna pattern of a 16-element linear array when the beam is steered 22° off boresight. *(Source: Gurgel et al., 1999.)*

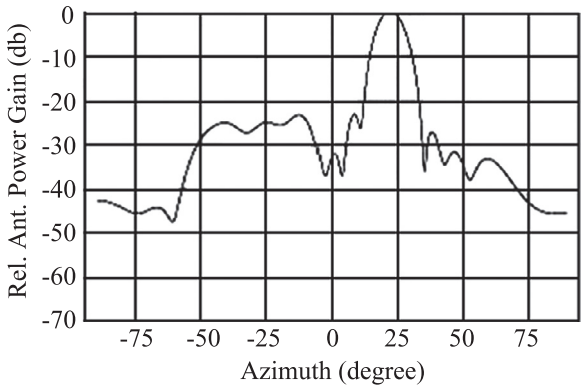

FIGURE 4.12 Same as Figure 4.11 but the pattern when the antenna is installed on real ground at an angle to the coastline. *(Source: Gurgel et al., 1999.)*

desired. Figure 4.12 shows the pattern of beams formed from a 16-element array when the array is set at an angle to a real coastline. Deviation of the pattern of beam from the ideal does not usually create problems in measuring currents, but it can cause corruption of some wave measurements. There is really no easy way around this problem, but the more compact the antenna array can be made, the smaller the effect, and it is now generally recognized that there is a need to develop such arrays (Gurgel et al., 1999).

It may be noted that only at HF (with a radar wavelength between 6 and 60 meters) can the sea echo be neatly decomposed. Microwave radars see an echo that is so complex as to be indecipherable in terms of the important underlying sea surface current information. In addition, HF radars with their long wavelengths see well beyond the visible horizon that limits all microwave radars. This is by virtue of the well-known rule that the lower the frequency, the farther the signal penetrates. If conventional radar wisdom is followed in forming and scanning a beam to derive bearing angle, the long wavelengths demand a huge coastal antenna facility. This has been the single major impediment blocking the acceptance of this tool by the ocean community, since it imposes large initial and operating costs, besides restricting the most obviously desirable site locations.

4.7. INSTRUMENTATION ASPECTS

Sea surface current mapping HF Doppler radar systems can be roughly divided into two types based on the method used to determine bearing to a sector of the ocean surface: (1) beam forming, or (2) direction finding. As mentioned earlier, beam-forming radars electronically steer a linear phased array of receive antennas toward a sector of sea surface; direction-finding radars exploit the directional properties of loop antennas to determine bearing. Digital signal processing and computing play a vital role in the operation of radio-wave pulse-Doppler radar systems used for mapping sea surface currents. The Doppler radar system consists of a transmit antenna, an array of receiving antennae, an antenna control and multiplexing unit, digital control, digital beam-forming and data-acquisition units, front-end data processing and archival modules, and online sea surface current estimation and data communication algorithms run on a computer. Data processing involves several steps, including Fourier processing of the radar echo signal, formation of narrow receiving antenna beams in several different directions by digital beam-forming techniques, and estimation of Doppler shifts of the backscattered signal from which radial sea surface current velocities can be estimated.

The transmitting antenna system radiates electromagnetic energy to the sea surface, usually using a wide-beam omnidirectional transmitting antenna, as a stream of continuous wave (CW) short bursts (i.e., pulses) of width τ (usually less than 20 μs) at every few milliseconds, to floodlight the survey area. Timing signals in the hardware, controlled by a computer, ensure coherence between the transmitter and receiver internal signals. A steerable narrow receiving beam is usually employed for the selection of the desired azimuth and directivity to achieve gain and for rejection of noise, interference, and sea echo from other directions (Shearman, 1986). The receiving beam can be steered in several directions by varying the relative complex weights applied to the signals emanating from each receiving element of the linear receiving antenna array. This permits velocity measurements in several directions. The beam formation is done in software in the frequency domain (Teague, 1986). Electronic steering of the receive beam becomes necessary because, in contrast to microwave radars, mechanically rotating an HF/VHF antenna is impractical due to its prohibitively larger size (see Figure 4.9).

In the receiver section, under computer control, the receiver gain is increased at an interval of τ to compensate for the decrease of echo strength with increasing range. This procedure, known as sensitivity time control (STC), is similar to the automatic gain control (AGC) commonly used in echo sounders and acoustic Doppler current profilers (ADCPs). In the receiving circuitry, after amplification, the echo signal is coherently mixed down in a mixer to produce an in-phase and quadrature (I and Q) intermediate frequency (IF) centered at 0 Hz (i.e., zero intermediate frequency). The mixing process demodulates the Doppler frequency-shifted echo signal (usually a few tens of megahertz) and provides an output signal that contains only the Doppler shift component (a few Hertz). The use of I and Q signals allows the separation of positive and negative Doppler shifts so that approaching waves can be distinguished from receding waves (Teague, 1986). After suitable amplification, the I and Q signals are digitized with a high-resolution analog-to-digital (A/D) converter every τ s (i.e., corresponding to each range gate). Subsequently, these signals are digitally filtered over $1/n$ seconds to reduce the signal bandwidth to n Hz. This

process filters out noise beyond this bandwidth, which originated from various natural and manmade sources, near-DC components, higher-order scattering components, spurious spikes due to interference, and so forth. The value of n is typically 2 to 4.

Because the radio signals backscattered by the sea surface consist of a pair of very narrow side bands displaced above and below the carrier frequency by a few Hz or a fraction of a Hertz at HF/VHF, this value of n easily accommodates the cumulative Doppler shifts in the received echo arising from the phase velocity of the sea surface waves and sea surface currents. A number of such digitally filtered complex samples (i.e., real part and imaginary part) for each range gate and each receiving antenna are then collected for N s and added together in an accumulator and averaged to improve the S/N ratio. These time-averaged signals are then input to a complex fast Fourier transform (FFT), thereby converting the time-domain signal into frequency-domain information, which reveals the Doppler shift of the backscattered echo frequency with reference to the transmitted frequency. The first-order echoes are extracted from the second-order continuum by first searching for the peak of the power spectrum in a narrow region centered on the theoretical position of the Bragg line. Then the nulls between the first-order peak and the second-order continuum on either side of the Bragg line are found by searching for the points at which the local slope of the smoothed frequency spectrum changed sign. The nulls thus define the limits of the first-order energy band. This technique has been successfully used by Teague (1986).

The displayed spectrum will then have a Doppler resolution of $1/N$ Hz over a window from $-n$ to $+n$ Hz, where N is the integration time. The $1/N$-Hz Doppler resolution yields a radial current velocity resolution of $\lambda_r/2N$ cm/s. For $N = 256$, a 25-MHz (i.e., $\lambda_r = 12$ m) Doppler radar provides a radial current velocity resolution of $\sim$2.5 cm/s.

The essence of data processing is to detect the centroid of the first-order spectrum (the first-order moment). The centroid is found by integrating the spectrum over the first-order energy band. The frequency corresponding to the centroid of the spectrum is taken as the frequency of the Bragg line. The surface-current-induced displacement (Δf) in the Doppler shift (see Figure 4.3) is determined by subtracting the theoretical Bragg frequency from the measured frequency. The difference (Δf) is converted to current velocity using the relation $V_{cr} = \dfrac{\lambda \Delta f}{2}$. The processing software also determines the range and bearing corresponding to each of the unique radial velocity estimates.

Although the backscattered energy from the Bragg scattering process is much larger than that from other reflections, in practice many observations must be averaged to obtain a statistically reliable estimate of the locations of the spectral peaks. Because of the requirement of a large spatial and temporal averaging, a single radar observation bin is usually of the order of 1−3 km wide and approximately 1 h in duration (Paduan, 1995).

A particular transceiver system (i.e., a pair consisting of a transmitter and a receiver) can measure only the radial components of currents with respect to an antenna from various range cells defined by the geometry of the transceiver system. To obtain an unambiguous map of two-dimensional sea surface current flow pattern at maximum resolution, it is necessary to obtain measurements from at least two radar systems located in different spatially distant locations. The use of two systems to determine radial currents at a given coordinate from two directions allows calculation of the resultant current speed and direction (i.e., total vector current).

To accomplish this, two separate radar systems (one master and one slave) are to be installed and positioned at a sufficiently large distance apart (typically 20−30 km). When the two radars are properly sited, their beams overlap over the survey area of the sea surface at sufficiently large angles to permit accurate estimation of sea surface current vectors at different surface bins (defined by a distinct range cell and angle section). Because each individual radar system measures the component of current along its line of sight, two radars together give unambiguous estimates of sea surface currents.

In practice, two sites at least 5 km apart are chosen. This is illustrated in Figure 4.13. During the sampling interval, the master radar system transmits, receives, and processes the backscattered energy and interpolates the information from each of the numerous grid points. This entire process is repeated several times over a few minutes. During this period, the slave radar system also transmits, receives, and processes its signals, followed by a few minutes of data reduction. Subsequently, slave data are sent to the master radar system's computer via a UHF radio link, to combine the radial currents gathered by the two radar systems into two-dimensional current vectors (speed and direction), store the time-series datastream, and display the sea surface current map on a video monitor. To accomplish this, the latitudes and longitudes of the two radar sites are entered into the master site computer, along with the azimuthal bearings of the two receiving antenna arrays. The software then converts the radar-oriented polar coordinates of each bin into rectangular coordinates. Details of this aspect may be found in Lipa and Barrick (1983) and Leise (1984).

If the signal from a given bin is too weak, the sea surface current velocity at that bin is usually calculated by interpolation from the adjacent range azimuth cells. Averaging hundreds of current maps enables the removal of random errors. The angular sectors very near the shore (i.e., baseline) are sometimes excluded because the nearly parallel radial velocities seen from each site at these grid points give rise to large vector errors. Baseline instability arises from the fact that the transverse velocity component cannot be sensed. Consequently, only one degree of freedom is measured and

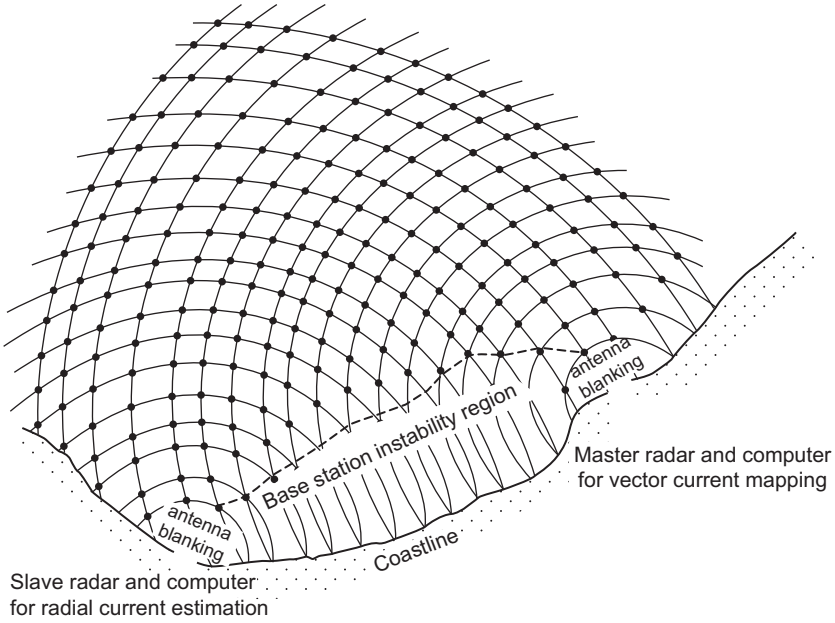

FIGURE 4.13 Conceptual rendition of the spatial coverage of dual-site HF/VHF Doppler radar systems using two wide-beam transmit antennas. The dots represent the locations on the sea surface from which radial water-current vectors are derived using echoes received at both the radars.

the vector inversion breaks down. Similar instability exists at large distances from the radar sites as well (Lease, 1984).

4.8. RADIAL AND TOTAL VECTOR CURRENTS

Two remotely located stations are required to measure the sea surface current vectors. By positioning the two stations so that beams from each of the two radar systems intersect near-orthogonally (Figure 4.14), sea surface current vectors can be accurately determined from the separately measured surface current velocity component directed toward or away from the radar, called the *radial velocity component*. The radial components of currents are monitored along various orientations from the radar. Along each beam, surface currents are measured in range bins of a certain radial and azimuthal dimensions (see Figure 4.8). Therefore, the two-dimensional (2D) surface current velocity vector magnitude and direction (v, θ) can be extracted by adding the two radial velocity components (v_1, θ_1) and (v_2, θ_2) obtained at each radar station as follows (Mantovanelli et al., 2010):

$$v^2 = v_x^2 + v_2^y \tag{4.26}$$

$$\theta = \tan^{-1}\left(\frac{t_y}{t_x}\right), \tag{4.27}$$

where v_x and v_y correspond to the components of surface current vector with velocity (v) along the x- and y-axis, respectively, and t_x and t_y are parameters given by:

$$t_x = v_1 \sin\theta_2 - v_2 \sin\theta_1 \tag{4.28}$$

$$t_y = v_2 \cos\theta_1 - v_1 \cos\theta_2 \tag{4.29}$$

$$v_x = t_x/\sin(\theta_2 - \theta_1) \tag{4.30}$$

$$v_y = t_y/\sin(\theta_2 - \theta_1) \tag{4.31}$$

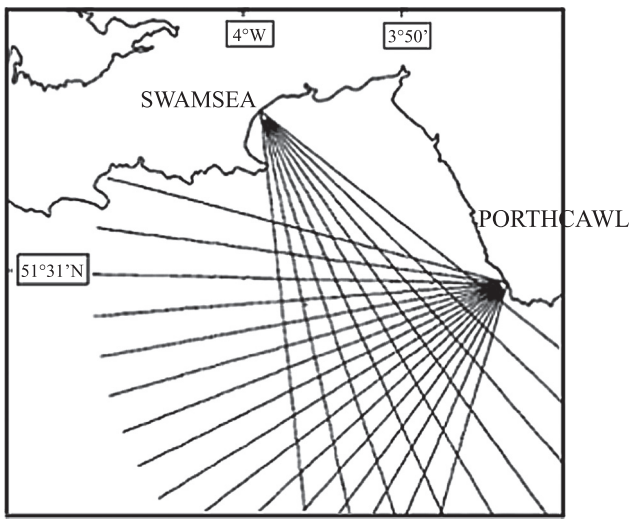

FIGURE 4.14 Positioning two radar stations so that beams from each radar intersect near-orthogonally. *(Source: Hammond et al., 1987.)*

4.9. DEVELOPMENTS ON OPERATIONAL SCALES

Subsequent to the pioneering theoretical and experimental accomplishments achieved by Crombie (1955, 1972), Wait

(1966), Barrick (1972), and Stewart and Joy (1974) on remote mapping of sea surface currents using the HF Pulse-Doppler radar system, the technique rose from an experimental to an operational stage when Barrick et al. (1977) designed and developed an operational HF radar system. This system could measure and map near-surface current vectors to ranges about 70 km from the shore. However, these ranges are usually affected by the attenuation of radio waves propagating along the sea surface, the scattering properties of ocean surface waves, and atmospheric radio noise. Both the attenuation and noise are strongly frequency-dependent.

On one hand, the attenuation of radio ground waves increases with frequency (Hill and Wait, 1980). On the other hand, the atmospheric (manmade) noise decreases above a certain frequency limit because of the absence of ionospheric reflection. At night, the S/N ratio is considerably larger than during daylight hours. However, during daylight hours, radio-wave interference reduces the possible range for current measurements to 25 km at 25 MHz (Essen et al., 1983).

The first commercial HF Doppler radar remote sensing system for measurement of sea surface current was the coastal ocean dynamics applications radar (CODAR). However, developments on HF radar, independent of CODAR, have been made in Canada at C-CORE (Hickey et al., 1995); in the United Kingdom at the University of Birmingham (Shearman and Moorhead, 1988); in France at the University of Toulon (Broche et al., 1987); in Australia (Heron et al., 1985); and in Japan (Takeoka et al., 1995). Based on CODAR (Barrick et al. 1977), further developments have been made in the United Kingdom by Marconi with the ocean surface current radar (OSCR) (Prandle et al., 1992). In the United States, CODAR was upgraded to SeaSonde (Paduan and Rosenfeld, 1996). Recently, the University of Hamburg developed a new system known as Wellen Radar (WERA) using frequency-modulated continuous wave (FMCW) techniques. The most popular systems among these are discussed in the following sections.

4.9.1. CODAR

The earliest system in operational use was the 25.6-MHz CODAR developed by Barrick et al. (1977). The original version of the CODAR system developed at NOAA transmitted short CW pulses within a wide beam and performed range resolution by means of the pulse length τ. In order not to disturb the receive signal, successive transmit pulses are separated by a period of the order of 100 τ. Because of the relative short transmit time, a high peak power is needed. The main advantage of this kind of range resolution is the simple technical design. The CODAR used a four-element square array (see Figure 4.7) with a direction-finding method for azimuthal resolution. The receiver processor used FFT routines to resolve equirange echoes within the beam, and the signals from the individual aerials (i.e., receiving antenna elements) were compared to estimate direction (Leise, 1984). Subsequently, estimates of radial current velocity versus range and bearing were constructed. A sample of sea surface currents mapped by CODAR is shown in Figure 4.15. Arrows represent current speed and direction; magnitude of current speed is indicated also by grey shading.

Researchers sought to reduce some drawbacks of a wide-beam system of the original CODAR by the use of a modified antenna system. This compact antenna system consists of three electrically separate elements, so excited that a beam of "cardioid" pattern on the sea surface is electronically steered to any angle in the horizontal (Figure 4.16). A single common steerable antenna system with the capability of transmission and reception, and meeting the stringent requirement of the compactness needed for deployment on offshore platforms, has been described as the most noticeable feature of the CODAR system. Paduan et al. (1995) reported an example of the complex nature of surface currents within and offshore of Monterey Bay as mapped by a multiple-site HF radar (CODAR) network.

While operating from off-shore oil rigs, the metals below the antenna affect the performance in two ways with respect to coastal installations (CODAR brochure). First, antenna patterns become slightly distorted by the metal directly below the antenna. For instance, Gurgel et al. (1986) observed that the ship-borne Doppler radar system's performance deteriorates as a result of the reflections of sea echo by the ship's metal. Second, the emitted radar signals getting into the metal structure of the rig can cause interference with other radio and TV equipment onboard if care is not taken during installation. The first problem is usually circumvented by measuring the actual antenna patterns by a radio source placed on a boat. The measured antenna pattern is then included in the inversion software as a lookup table. Barrick and Lipa (1986) discussed correction for distorted antenna pattern. The interference problem is usually handled by high-power bandpass filters at the transmitter output.

4.9.2. OSCR

An essential requirement in the use of radio-wave pulse-Doppler radar systems for measurement of sea surface currents is that the first-order peak in the echo spectrum must be identifiable from the higher-order continuum surrounding it. This requirement is always satisfied for a narrow receiving beam radar because the radar cell size on the sea surface is sufficiently small that the radial current variation across it is minimal. An important advantage of

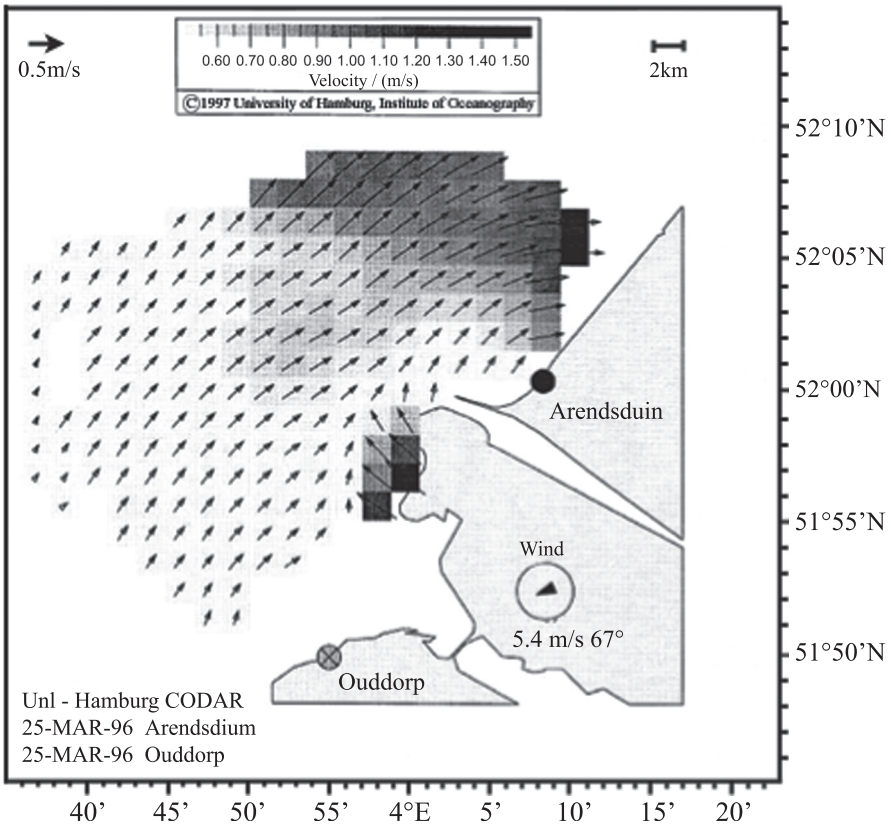

FIGURE 4.15 Sea surface currents mapped by CODAR**.** Arrows represent current speed and direction; magnitude of current speed is indicated also by grey shading. *(Source: Gurgel et al., 1999.)*

using a narrow-beam antenna instead of a wide-beam antenna is that the direction and range of the cells can be accurately determined (Eccles, 1989). Reception of a narrow beam of a pulsed, coherent radio wave in a known direction ensures that the direction of the radial sea surface flow component is precisely known. Based on these considerations, a number of systems are operational in various countries. These include the ocean surface current radar (OSCR), which originated at the Rutherford-Appleton Laboratory in the United Kingdom and was further developed by MAREX Ltd.

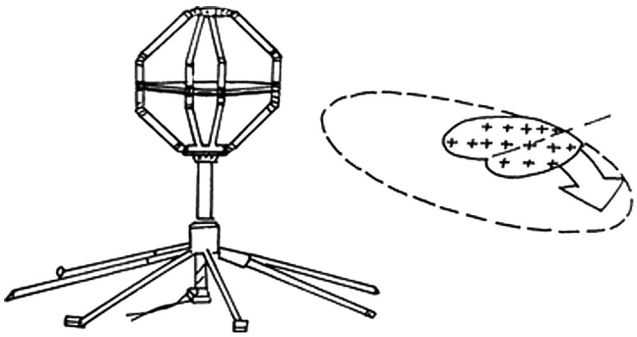

FIGURE 4.16 Compact antenna system used in CODAR. *(Source: CODAR Ocean Sensors brochure.)*

The system was designed to operate in one of two frequency ranges: 27 MHz (HF) for ranges approaching 35 km, and 51 MHz (VHF) for high-resolution measurements for ranges approaching 15 km. In the 51-MHz mode, the range cell size is a factor of 8 smaller than that used at 27 MHz, thereby improving the spatial resolution by this factor. The OSCR also transmits a wide beam but differs from the CODAR approach in using an 85-m-long, 16-element (for HF) or 32-element (for VHF) switched delay line matrix to form a phased-array antenna to achieve a narrow receive beam, which is electronically steered over the illuminated ocean surface area. In such pulse-Doppler radar, the angular resolution is controlled by the length (in wavelengths) of the phased array that is used for signal reception. An antenna configuration employing a long phased array and digital beam-forming techniques can "point" the radar (Figure 4.17). The beam width is a function of the radar wavelength divided by the length of the phased array, which is approximately 8° for the HF mode of OSCR. With a beam dwell time of approximately 2 min, the sea surface current resolution is approximately ±1 cm/s within cells of typically 1.2 $R\Theta$ km, where R is the range and Θ is approximately ±0.1 rad. The OSCR system could achieve these improvements in terms of accuracy (2 cm/s for radial current and 4 cm/s for total vector current) and

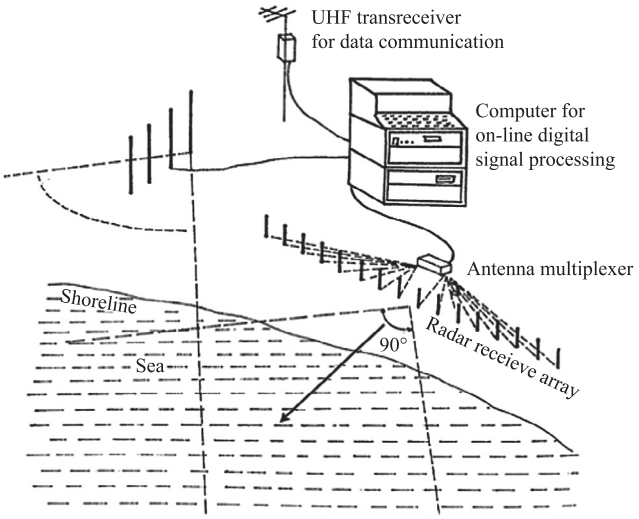

FIGURE 4.17 A typical configuration of OSCR transceiver system. *(Source: In part from an OSCR brochure.)*

spatial resolution (1 km) due to the use of a narrow-beam receive array by enhanced digital beam-forming techniques. The accuracy is a function of the spectral resolution, angle of intersection between the master and slave radial beams, and the positioning accuracy of the antennas. Other effects such as atmospheric noise and sea echo may induce additional uncertainty in the velocity field or limit the range performance (Barrick, 1980).

Figure 4.18 shows a map of sea surface current distribution in the Dover Strait produced by an OSCR system. The OSCR system has no ambiguities and offers better resolution than does the CODAR, although the shore station requires greater space and is less portable.

To achieve the best possible result from radio-wave pulse-Doppler radar systems, a lot of care needs to be taken in their installation. The radar location needs to be chosen so that the antenna has an unobstructed view without being shadowed either by buildings or hills. The antenna should be located as close to the water as possible, preferably within 50 m. Barrick et al. (1977) found that the optimal location for the antennas is at sea level on the beach, as close to the water as possible, with the grounding system beneath the antennas making electrical contact with seawater. Land of greater extent than 100 m severely attenuates the signal. This observation was supported by Lane et al. (1999), who noticed in their field measurements in the U.K. waters that analysis of the OSCR data gave good results for the cells nearest the radar sites, but the data return and associated quality decreased with increasing range, especially close to the Northern Irish coast where the water is shallow and there are small islands present. There appeared to have been localized interference from a nearby broadcast transmitter.

4.9.3. SeaSonde

The SeaSonde, manufactured by Codar Ocean Sensors, Ltd., Los Altos, California, evolved out of the original CODAR developed by NOAA's Wave Propagation Laboratory (now

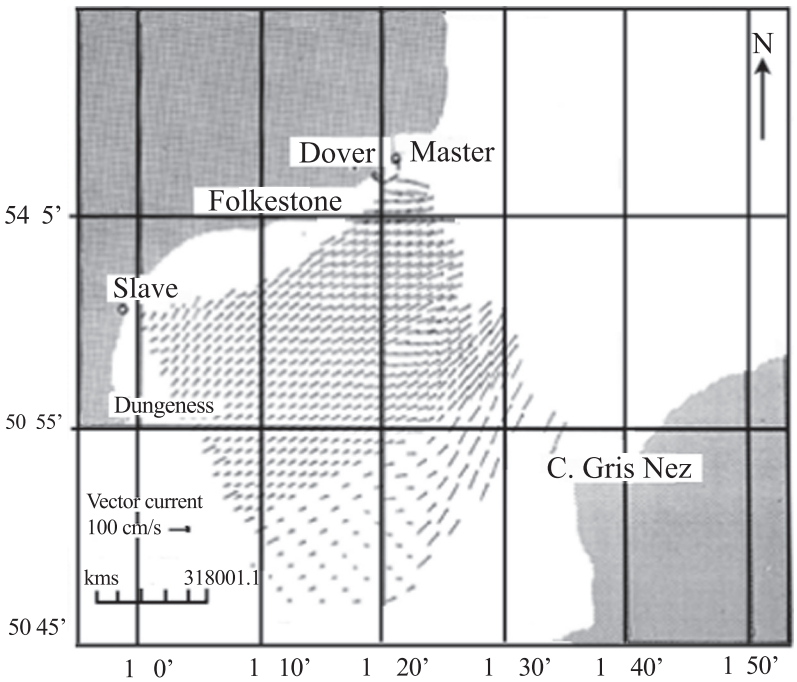

FIGURE 4.18 Map of surface current distribution in the Dover Strait produced by OSCR system. *(Source: Collar, 1993, reproduced with kind permission from National Oceanography Centre, Southampton SO14 3ZH, United Kingdom.)*

the NOAA Environmental Technology Laboratory). The CODAR SeaSonde system uses a three-element crossed-loop/monopole receive antenna along with a variant of the multiple signal classification (MUSIC) algorithm (Schmidt, 1986) to determine bearing. This configuration allows a deployment in a smaller area compared to a phased array antenna system. However, the system may be more sensitive to antenna response patterns, and the effect of this on surface current data is not well documented.

Historically, sea surface current-mapping direction-finding (DF) antennas and algorithms have taken several forms. Barrick et al. (1977) and Gurgel (1997) used linear array antenna elements separated by short distances and relied on phase-path differences to extract bearings. On the other hand, as old as radio itself, the simplest DF system is a loop antenna rotated until the incoming signal vanishes. Knowledge of this null direction and the angular response function of the antenna provides information about the direction from which the radio signal is originating. The most compact realization of DF techniques for this purpose has been the CODAR-type HF radars, which employ two crossed loops mounted around a whip (a vertical monopole). Such an antenna configuration is shown in Figure 4.19, along with stylized plots of the ideal angular amplitude patterns for each of the three elements. In addition to the theoretical (and achieved) shape of the antenna patterns, the accuracy of all DF algorithms also depends on the S/N ratio of the measured backscatter.

SeaSonde is an enhanced version of CODAR. Like CODAR, the SeaSonde overcomes the obstacle of requiring a huge coastal antenna facility with the use of compact antennas that rely on direction finding rather than beam forming. The receive antenna system is mounted up on a post, out of reach, or on the roof of a building rather than sprawling over hundreds of meters of valuable seafront property at the shoreline. This, combined with a novel, highly efficient patented waveform that works well at HF, allows the SeaSonde to be very compact and portable. This system uses the frequency-modulated interrupted continuous wave (FMICW) technique for range resolution. Azimuthal resolution is achieved by a very small loop antenna combined with a special direction-finding algorithm. Controlled by unattended desktop PCs, real-time files are sent to the desired user office. There they are combined with similar data from other SeaSondes viewing the same area from tens of kilometers away to produce total vector fields. Typically they generate hourly current maps, and often data are automatically uploaded to Web sites for immediate access by the public.

The standard SeaSonde operates between 12-27 MHz to ranges of 30−60 km with typical resolution of 1 to 3 km. The Hi-Res SeaSonde provides 200−500-meter range resolution over bays with smaller areas such as 10−15 km. The latest addition is the Long-Range SeaSonde, achieving average daytime ranges of 170−200 km. The Long-Range SeaSonde makes it possible for a country to map currents along large sections of its coastline, continuously, with low initial and operating costs.

Rutgers University operates four Long-Range SeaSonde radars. They monitor the entire continental shelf off New Jersey. The current vectors are averaged and overlain on satellite-derived AVHRR sea surface temperatures. The SeaSonde can provide near-real-time data updates, even when satellite data are unavailable due to cloudy weather or other reasons.

At present, SeaSondes are used worldwide to monitor coastal sea surface currents to as far as 220 kilometers offshore. This has proven to be one of the technologies for emerging coastal ocean observing systems. HF Doppler radar is also making an impressive contribution to ocean forecasting programs.

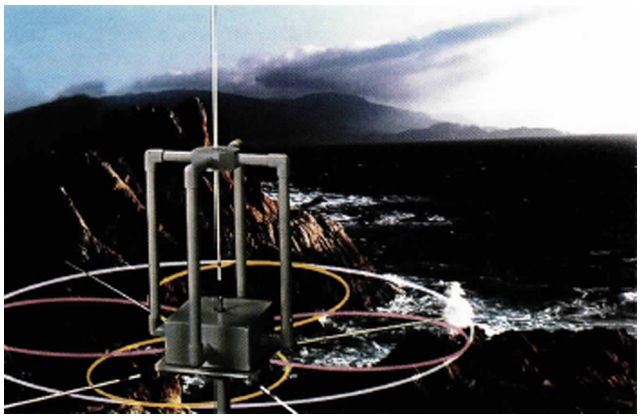

FIGURE 4.19 Stylized view of a coastal SeaSonde crossed-loop/monopole receive antenna. Indicated at the antenna base are idealized patterns of the two loops (yellow and pink) and the vertical whip/monopole (white). *(Source: Barrick and Lipa, 1997.)*

4.9.4. WERA

Wellen Radar (WERA) is a new HF radar developed at the University of Hamburg, Germany. WERA uses frequency-modulated continuous wave (FMCW) chirps (without transmit/receive switching) instead of CW pulses. Chirp waveform and some of its specialties are given in chapter 12. One main advantage of this system is the possibility of connecting different configurations of receive antennas. WERA can be operated with up to 16 receive antennas. When operated with such a linear array, information on the sea state can also be obtained via second-order spectral bands. The capability of measuring surface wave spectra by means of WERA has been discussed by Wyatt et al. (1999). A further advantage is the flexibility in range resolution between 0.3 and 1.2 km instead of a fixed resolution of about 2 km for CODAR. In addition, because both transmitter and receiver operate continuously, the "chirp" technique avoids the blind range of about 3 km in front of

the CODAR. Range resolution by means of FMCW chirps requires a more advanced technique than the resolution by means of CW pulses. However, the chirp method is advantageous in several aspects. It allows more flexibility in altering transmit frequency and range resolution. In particular, the S/N ratio can be improved by avoiding aliasing problems, and it should be possible to increase the currently realized working range.

HF radars transmit electromagnetic waves to the sea surface and record the backscattered signal, which contains information on surface current and waves. To locate the scattering area, spatial resolution has to be achieved in range and azimuth. Unlike all other HF Doppler radar systems described before, WERA transmits linear-frequency chirps. The range cell extent is related to the bandwidth of the chirp. The transmit signal is:

$$s(t) = \sin\left[2\pi\left(v_o + \frac{b}{2T}t\right)t\right], \tag{4.32}$$

During the chirp period T, the frequency (i.e., the derivative of the phase with respect to time) linearly increases from v_o to $(v_o + b)$. After reaching the maximum frequency, the chirp is repeated. The received signal is a superposition of HF waves, which have been backscattered at different distances from the radar. Range resolution is performed by Fourier transforming each single chirp. The resolution of the frequency $v = b\tau/T$ is determined by the length T of the chirp such that $\Delta v = 1/T$. Thus, the resolution of the propagation time $\Delta\tau$ and, in turn, range Δr becomes (Gurgel et al., 1999b):

$$\Delta\tau = \frac{T\Delta v}{b} = \frac{1}{b}, \quad \Delta r = \frac{c}{2}\Delta\tau = \frac{c}{2b}, \tag{4.33}$$

where c is the speed of light. It should be mentioned that the Fourier transform requires some caution. Due to the leakage problem in spectral analysis, near-range high-energy spectral lines may mask far-range lines of low energy. This problem is accounted for by applying a window filter to the chirps prior to the Fourier transform.

Advantages of range resolution chirp technique are the possibility of altering the range cell extent by simply modifying the width of the chirp, omitting the blind range in front of the radar, and a lower data rate to be processed in the receiver. However, transmitter and receiver must be designed for extreme dynamic range and linearity, since the superimposed near-range high-energy and far-range low-energy signals have to be separated.

The most crucial component of FMCW radar is the chirp generator. Advantages of the direct digital synthesizer (DDS) WERA uses are high flexibility and optimum realization of a linear chirp at low phase noise. The chirp is used by both transmitter and receiver. A block diagram of the hardware is presented in Figure 4.20. The DDS is controlled by a high-speed counter. Start and stop frequency can be

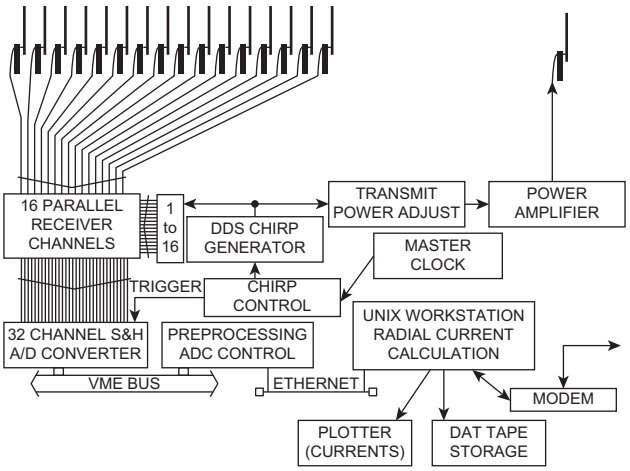

FIGURE 4.20 Block diagram of WERA system. *(Source: Gurgel et al., 1999.)*

changed easily, which permits modification of mean carrier frequency and range resolution. The system master clock is a stable synthesizer. Its long- and short-term stability and low phase noise are essential for good performance.

In WERA the generated chirp is split into 17 channels. One controls the transmitter. The others are needed for the phase-coherent I/Q demodulation of the backscattered signals. This is performed by 16 independent direct-conversion receivers connected to the receive antennas. Before A/D conversion, a low-pass filter suppresses the frequencies above the Nyquist frequency, and a high-pass filter attenuates the strong signals received directly from the transmit antenna. The measured characteristics of the filters are compensated for by software during data analysis. To extend the dynamic range of the 16-bit A/D converter, the signal is oversampled 13 times. The next steps of signal processing are implemented in software.

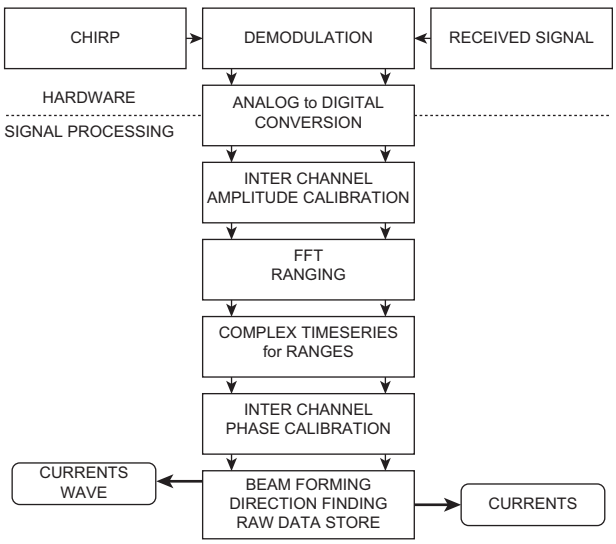

FIGURE 4.21 Signal processing implemented in WERA. *(Source: Gurgel et al., 1999.)*

Figure 4.21 illustrates the signal processing implemented in WERA. After A/D conversion of the complex demodulated signal, an interchannel amplitude calibration is applied to compensate for gain variations of the 16 receivers. Range-resolving FFT is then applied to all channels. A windowing function, as described by Gurgel et al. (1999a), has to be used in this context. After sorting the data into range cells, the complex time series are available. An interchannel calibration of the phase is performed and the data are stored for further processing. Amplitude and phase calibration are crucial for the accurate performance of azimuthal resolution techniques.

4.9.5. Systems for Special Applications

In addition to the systems described thus far, a few others have been developed for special applications (Gurgel et al., 1999b). The Pisces radar is one among them. Pisces is based on the FMICW technique for range resolution. Beam forming is provided in hardware by switchable cables used as phase shifters. FMICW introduces transmit/receive switching to overcome dynamic range limitations.

Another system is the C-CORE Cape Race. This system provides a high azimuthal resolution by a 40-element linear array, which is some 1 km long. This is a very large permanent installation for research, namely, tracking icebergs.

The Australian coastal ocean surface radar (COSRAD), developed at James Cook University, is operated at 30 MHz and uses pulses of 20 μs duration, yielding 3-km range resolution. In contrast to the other systems mentioned, which perform illumination of the measurement area by a wide-angle transmit antenna, a common antenna array for transmit and receive is used to perform beam forming. This has the advantage of squared side-lobe directivity performing a narrower beam, and this scheme increases the S/N ratio. However, because the different directions are scanned step by step, the azimuthal surveillance is slow, and technical problems in switching the antenna between transmitter and receiver arise.

Another pulsed Doppler radar system is the Courants de Surface MEsures par Radar (COSMER). This VHF system is a radio-oceanographic instrument developed by Laboratoire de Sondages Electromagnetiques de l'Environnement Terrestre (LSEET), University of Sud-Toulon-Var, France (Broche et al., 1987). It includes two Doppler radars, set on the coast, operating respectively at 45 and 47.8 MHz. The radars are operated with a linear phased array of eight receive whip antennas parallel to the coast (total length: 25 m or 50 m for 16 antennas) and with a transmitting network of four whip antennas perpendicular to the coast (total length: 12 m). The radars operate in pulsed mode, with a pulse width of 4 μs and a pulse repetition rate of 200 μs. The maximum range is 30 km. Both radars measure the radial components of the current in the range direction, at all the sampled distances, with an azimuth resolution of 14° (with eight antennas, beam-forming processing). The radar derives vertically averaged quantities over 25 cm (at 50 MHz) and temporally averaged over 9 minutes (Cochin et al., 2006).

4.10. INTERCOMPARISON CONSIDERATIONS

No measurement is complete without its error bars; therefore, uncertainty estimates are indispensable in comparing different datasets. Understanding the data involves clear insight into uncertainties as well. In attempting intercomparison among different instruments that measure a given parameter, it is necessary to clearly understand the way each instrument measures that parameter.

Several studies of sea surface current measurements made remotely by HF Doppler radar systems have validated the fundamental schemes embodied in them through comparisons with *in situ* measurements. Seminal studies by Stewart and Joy (1974), Barrick et al. (1977), and Frisch and Weber (1980) verified the underlying physics of the HF Doppler radar-based integrated surface current measurements by comparisons with Lagrangian drifters. These were soon followed by Holbrook and Frisch (1981), who compared the output of the CODAR system with records from a vector averaging current meter (VACM) moored at 4, 10, and 20 m depth; Janopaul et al. (1982), who intercompared three different radar systems with instruments at 7 and 10 m depth; and Schott et al. (1986), who included comparisons between direction-finding HF Doppler radar systems and moored current meters. Collar and Howarth (1987) compared data from the OSCR Doppler radar system with corresponding observations made by surface current buoys measuring at 1 m depth. Such comparisons have limitations, in part because the radar and current meters are responsive to different horizontal scales of motion, although use of a small current meter array distributed through a radar cell can improve matters (Collar, 1993).

More fundamentally, the radar senses a depth-integrated current, whereas the current meter samples at a point. Furthermore, in virtually all experiments reported, the moored instruments have sampled well below the effective mean depth of the radar and cannot therefore be expected to record the same current when the current structure is strongly sheared with depth under the influence of wind stress. The weight of evidence from studies conducted by the Institute of Oceanographic Sciences (IOS) in the United Kingdom has confirmed that the mean depth of response for radars operating at 27 MHz lies within 1 m of the sea surface. There is also the view that the radar includes a contribution from Stokes Drift in its measurement.

Finally, the point should be made that in making comparisons in shallow coastal waters, it may be necessary

to make allowance for the current shear in the bottom boundary layer (Collar, 1993).

Several simultaneous observations have been made also using Doppler radar and surface drifters (Barrick et al., 1977; Ha, 1979; Collar and Howarth, 1987). Drifters can be drogued so as to follow the local water mass at depths commensurate with the radar averaging depth, though care is required in drogue design. Agreement between the two techniques to within a few cm/s has been reported in several of the studies, although mostly in relatively calm conditions, in which variability within the radar footprint almost certainly provides the ultimate limitation.

Hammond et al. (1987) reported results of intercomparison of current speed and direction outputs between OSCR and rig-mounted Aanderaa current meters. The study was carried out within an area of high tidal currents and complex bottom topography, located along the northern coastline of the Bristol Channel, U.K. Compared with simultaneous data obtained from conventional self-recording current meters, the radar measurements of surface currents were to within 5−10% in speed and 10° in direction. Thus, it was found that in the absence of wind influence, excellent agreement between the various techniques for measuring current speed and direction is the characteristic of the majority of the outputs (Figures 4.22 and 4.23). The OSCR data, which represent currents at the air-sea interface, were the highest of the set; they were in reasonable agreement with the speeds recorded by the upper meters on each of the rigs. However, substantial differences between the two datasets (i.e., OSCR and current meters) were found during short-term changes in the superimposed wind field.

Further studies such as Shay et al. (1995), Graber et al. (1997), and Chapman et al. (1997) built on earlier works by comparing OSCR measurements with a variety of moored and shipboard measurements. These studies increased the understanding of errors and limitations present in all HF

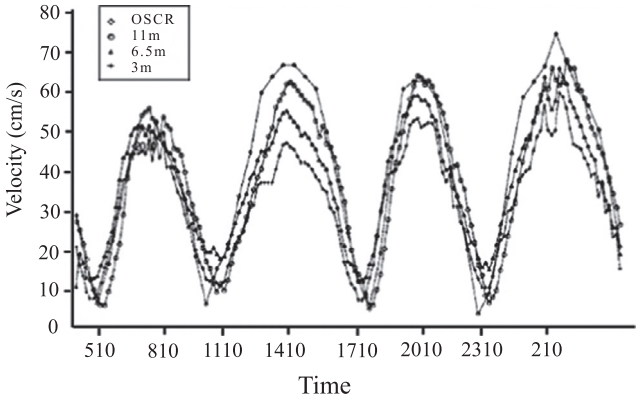

FIGURE 4.22 Intercomparison of current speed outputs from OSCR and self-recording current meters moored at 3, 6.5, and 11 m above the seabed. *(Source: Hammond et al., 1987.)*

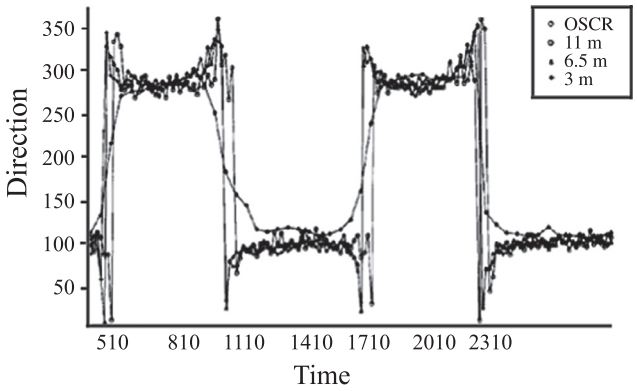

FIGURE 4.23 Intercomparison of current direction outputs from OSCR and self-recording current meters moored at 3, 6.5, and 11 m above the seabed. *(Source: Hammond et al., 1987.)*

Doppler radar current measurements, but fewer studies of CODAR SeaSonde employing MUSIC algorithm for direction finding were available. Exceptions include Paduan and Rosenfeld (1996), who reported comparisons of total vector currents that combined data from newer SeaSondes and an older CODAR HF radar; Hodgins (1994), who reported comparisons with drifters as well as modeled currents; and subsequently Kohut et al. (1999) and Paduan et al. (2001). Studies by Emery et al. (2004) sought to add to the understanding of the CODAR SeaSonde and its MUSIC direction-finding algorithm based on comparisons with an array of nine moorings in the Santa Barbara Channel and Santa Maria basin deployed between June 1997 and November 1999. Eight of the moorings carried vector-measuring current meters (VMCMs), and the ninth had an upward-looking acoustic Doppler current profiler (ADCP). Coverage areas of a network of five CODAR SeaSonde HF Doppler radar systems (broadcasting near 13 MHz and using the MUSIC algorithm for direction finding) and moorings included diverse flow and sea-state regimes. Measurement depths were ∼1 m for the radar systems, 5 m for the VMCMs, and 3.2 m for the ADCP bin nearest the surface. Comparison of radial current components from 18 radar-mooring pairs yielded rms speed differences of 7−19 cm/s and correlation coefficients squared (R^2) in the range of 0.39−0.77. Noise levels corresponding to 6 cm/s rms were evident in the radar data. Errors in the radar-bearing determination were found in 10 out of 18 comparisons, with a typical magnitude of 5−10° and a maximum of 19°. The effects of bearing errors on total vector currents were evaluated using a simple flow field and measured bearing errors, showing up to 15% errors in computed flow speeds and up to ∼9° errors in flow directions.

Lipa (2003) carried out field intercomparison studies between SeaSonde radar and ADCPs, which are two different kinds of modern instruments for remote (i.e., noncontact) measurements of ocean currents. These two

instruments function in different ways, although they measure the same oceanographic parameter. Many sources of uncertainty in SeaSonde velocities are familiar, such as statistical variation, nonoptimal analysis parameters, etc. In addition, each radar cell contains different current velocities due to horizontal velocity shear on the ocean surface. Such instances are often encountered in the oceanic upper layer because in a variety of oceanic regions, this layer often encompasses very strong and extremely variable currents (e.g., jets, eddies, meanders, filaments, etc.). Such energetic features have presented major risks for marine operations and have caused costly losses of structures over various areas of the world. The HF radar averages over these variable current velocities, and therefore any of these values may apply at a single point within the radar cell. The standard deviation of these individual velocities may be referred to as *spatial uncertainty* (Lipa, 2003). Thus, when HF radar (spatial average) and point measurements are compared, discrepancies are bound to exist in the presence of current shear.

Spatial uncertainty in the SeaSonde HF radar average can be estimated, however. During data processing, the radial velocity value is defined by the signal frequency, and analysis of the antenna voltage signals yields the corresponding direction of arrival. Usually, several velocities fall within a radar cell, and their standard deviation is a measure of the spatial uncertainty, which tends to increase with range from the radar along with the size of the radar cell. Even if the spatial uncertainty is high, the uncertainty in the average can be low. Thus, SeaSonde HF radar measurements appear stable from time to time, and two SeaSonde HF radars operated side by side will produce similar results. However, it can be a different matter when a SeaSonde "area measurement" is compared with an ADCP "point measurement." In the presence of sizable velocity shear, good agreement between the two measurements can be expected only if the radar cell size is small. Poor agreement does not necessarily indicate inconsistency if the differences are less than the error bars (Lipa, 2003). Lipa suggests that in comparing HF radar (SeaSonde) and ADCP data, it is best to compare radial velocities, resolving the ADCP velocities into components radial to the radar site. Then, differences between measurements can be compared with the radar uncertainties, which are different for each of the two radar systems. Individual uncertainties are lost when radial velocities from two sites are combined to form resultant velocities, and therefore comparing resultant velocities is not as informative.

Lipa (2003) provides the so-called *baseline test* as another example of SeaSonde velocity comparisons. A baseline test is a consistency check on radial velocities from two SeaSondes at points on the baseline joining the two sites. Because the SeaSondes "see" the same radial current along the baseline, the two systems will ideally give the same estimates of radial velocity. However, at all baseline points except the midpoint, the sizes of the radar cells differ, and spatial uncertainty may play a role.

Lipa (2003) has reported baseline tests performed on SeaSondes at Montauk and Misquamicut on the Long Island Sound. It was found that the Montauk and Misquamicut rms radial speeds differed by as much as 40 percent on the baseline near Montauk. This discrepancy was found to be due to the different radar cell sizes and the large velocity shear close to Montauk, where the current swirls around Montauk Point. Because the radar cell size is proportional to the distance from the radar, the cell sizes for Montauk in this region are much smaller than for Misquamicut. A smaller cell size results in less averaging-down of the velocity. Thus, the Montauk site produces current velocities with higher values and lower spatial uncertainties. The large baseline deviations are completely accounted for by the large spatial uncertainties in the Misquamicut data.

Based on this discussion, it may be concluded that in comparing sea surface current velocity measurements, it is not sufficient to simply compare the values; the uncertainties also need to be considered. For the area-averaged measurements produced by HF radar systems, uncertainty estimates should include uncertainties due to horizontal velocity shear on the sea surface. Surface current velocity measurements from two instruments can be considered to be consistent if the differences are within the uncertainty limits.

Intercomparison experiments of land-based HF Doppler radar systems against *in situ* and remote measuring subsurface devices have been addressed so far. It is worth examining the results of intercomparison measurements from different makes of HF Doppler radar systems. Gurgel et al. (1999b) reported such studies between CODAR (which achieves azimuthal resolution using direction finding in Fourier domain) and WERA (which achieves azimuthal resolution using a beamforming method). Both CODAR and WERA systems were installed at two sites north and south of the Rhine estuary mouth. The CODAR was equipped with the four-antenna square array; the 16 receive antennas of WERA were separated into a 12-antenna linear array and a four-antenna square array.

Figure 4.24 shows radial speeds measured by CODAR (triangles) and WERA (crosses) at two different positions, A and B, in the Rhine mouth. The time series extended over two M2 tidal cycles with ½ h sampling. At position A, both measurements agree well with an rms difference of less than 5 cm/s. At position B, the CODAR measurements revealed some spikes within the almost continuous time series, whereas the WERA time series was stable. Position B is situated within the main shipping route toward Rotterdam harbor. For this reason, it was concluded that

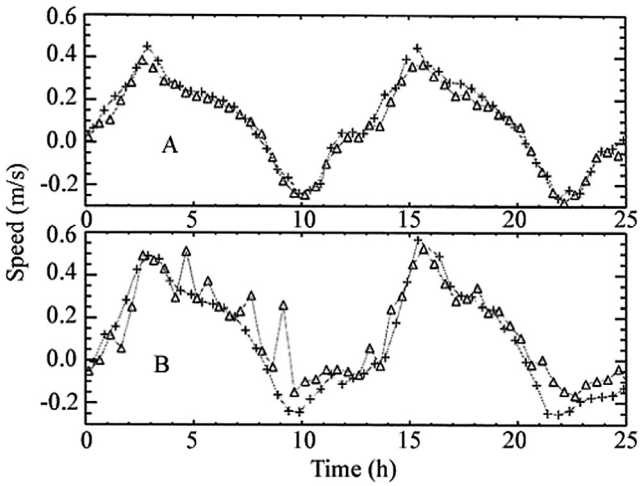

FIGURE 4.24 Radial speeds measured by CODAR (triangles) and WERA (crosses) at two different positions A and B in the Rhine mouth. *(Source: Gurgel et al., 1999.)*

the CODAR direction-finding algorithm is less robust than beam forming with respect to perturbations by ship traffic. This finding was confirmed by investigations of the S/N ratio of both measurements (Gurgel et al., 1997).

With regard to HF Doppler radar systems, it is worth noting that the maps of ocean surface currents are incomplete in space and time for the following reasons (Kim et al., 2007): (1) the algorithm on the measured Doppler spectrum does not provide a solution for all bearing angles; (2) the estimate of current vectors along the baseline between two radars where the measurements of radial velocities are nearly aligned suffers from poor geometric dilution of precision (GDOP) and frequently results in spurious total vector currents; the region with radial velocities crossing at angles less than 15−20° between two radars is commonly considered to produce unusable current vectors; and (3) hardware or software problems can lead to the temporary shutdown of individual radar sites. For example, Lane et al. (1999) reported that operational difficulties were experienced at the slave site of an OSCR system at Crammag Head (U.K.), where power failures occurred repeatedly and the system failed to reboot at times. Consequently, the data return over the 15 months of recordings was 62 percent.

In comparing surface current measurements using different technologies, the merits and limitations of each technology need to be taken into account. Major differences between surface current velocities from HF radar and other platforms are the following (Pandian et al., 2010):

- Measurements from HF radar, drifters, and current meters are all inexact. The frequency resolution of computed radar cross-spectra, which depends on FFT length, limits radial velocity resolution to ∼5 cm/s and 2.5 cm/s for 12 MHz and 25 MHz systems, respectively. Drifters can slip at ∼1 to 2 cm/s from the seawater parcel they follow (Ohlmann et al., 2005).
- Vertical scales of measurement differ. The HF radar gives vertically integrated values from the surface; drifters give integrated values over their drag elements; and current meters give values for specific depths (in the case of Eulerian current meters) or depth bins (in the case of ADCP).
- Horizontal scales of measurement differ. Typically, HF radars average over extensive horizontal areas (up to several km^2), whereas other platforms give point measurements or limited spatial measurements following motion.
- Measurements are not necessarily coincident in time, and Stokes drift may not be reconciled consistently among platforms (Ohlmann et al., 2007).

The plus point about HF Doppler radar networks is that despite several limitations, the two-dimensional maps of sea surface currents they provide represent a useful and unique resource for the improvement of coastal ocean circulation models, particularly in the critical depth range encompassing the euphotic zone (Paduan and Shulman, 2004).

4.11. ADVANTAGES OF RADIO-WAVE DOPPLER RADAR MEASUREMENTS

The main attraction of the coastally located Doppler radar technology lies in its ability to rapidly produce real-time two-dimensional maps of sea surface current distribution over a wide area in a way that would be difficult and prohibitively expensive using conventional instrumentation. It is thus especially useful in mapping flow patterns and their characteristics in waters around headlands, islands, or in estuaries. Experiments by several researchers have demonstrated the feasibility and practicality of mapping bay and estuarine flow patterns using land-based Doppler radar systems. Being a land-based system, sea operations are avoided, thereby enormously reducing weather dependence and other limiting factors. Sea surface current measurements using Doppler radar systems have some unique advantages over conventional methods of measurement. Probably the most important among them is its capability for remote measurements in time as well as space domains. This enables detection and mapping of time-varying as well as space-varying events such as gyres and complicated current structures, as demonstrated by Barrick et al. (1985) and Gurgel et al. (1986). It could also reveal fine structures of near-shore circulation (Prandle, 1987). Using Doppler radar, Shay et al. (1998) could obtain a unique view of the development and dissipation of complex features and spatial variabilities in the sea-surface circulation, such as mesoscale eddies and convergence

zones on a shelf, associated with a meandering western boundary current.

Another noteworthy feature of the Doppler radar technology is its inherent ability to measure currents without discriminating against Stokes drift (Barrick, 1986). The surface drift current has two components: (1) the shear current generated by the wind stress and (2) the Stokes current, which is related to wave statistics such as the phase velocity and height and length of the waves. Because the Stokes transport varies between 5 and 13 percent of the total surface drift (Wu, 1975), its inclusion in surface-current observation systems is clearly desired. Because most of the conventional sea surface current measuring devices, such as near-surface moored current meters, exclude Stokes surface transport, the inherent capability of the radio-wave Doppler radar systems to measure the total surface drift current is an added advantage. Results of sea surface current surveys in coastal waters and estuaries can be used to develop computer models that would assist in antipollution measures. Thus, Doppler radar systems can play a leading role in major investigations designed to help protect the marine environment.

A remarkable feature of the Doppler radar system is its ability to measure sea surface current shear at the topmost layer of the sea surface. This capability stems from the fact that the phenomenon of Bragg resonance, used for sea surface current measurements, occurs when a constituent of the predominant sea surface waves has a wavelength equal to one-half the radio wavelength of the radar. The sea surface wave trains contain numerous linear waves of differing wavelengths. Thus, with the use of multifrequency radars (3−50 MHz), it is possible to measure vertical current shear within the uppermost few meters of the ocean surface. This is a measurement that is very difficult to make by any other means.

Since their introduction in the 1970s, Doppler radar systems have been used extensively to deduce information on synoptic sea surface currents to ranges about 70 km from the shore (Barrick et al., 1977; Stewart and Joy, 1974; Frish and Weber, 1980; Georges, 1981; Prandle and Ryder, 1985; Prandle, 1987; Mathews et al., 1988; Parker, 1989). The radar system has the capability to cover vast areas of high shipping and fishing activities, where other methods would be impractical for long-term monitoring of sea surface currents. For example, under an Anglo-French collaborative research program with the leadership of the Proudman Oceanographic Laboratory (U.K.) to gauge the Dover Straits' capacity to transport waterborne pollutants into the North Sea, a master-slave pair of Doppler radar systems on the British coast was effectively used in tandem with a second pair on the French coast. Between them, the two radars could monitor sea surface current flows across the entire width of the strait at a spatial resolution of 1 km. This monitoring program exemplifies the advantages of Doppler

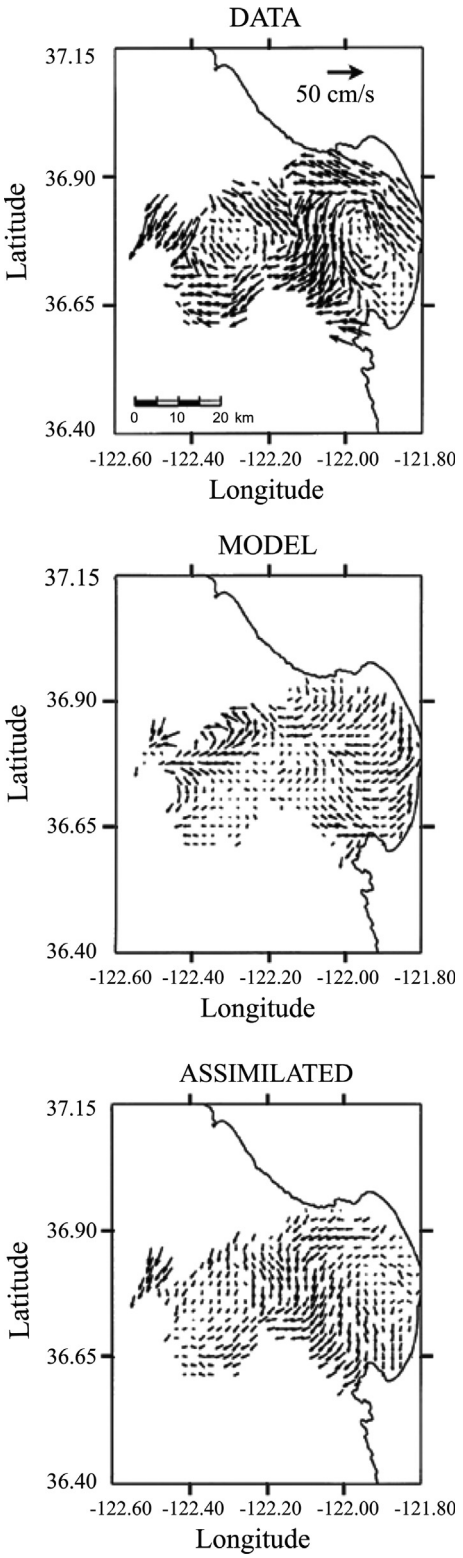

FIGURE 4.25 Pattern of surface currents as determined by HF Doppler currents (top), the numerical ocean model without any assimilation of the Doppler current (middle), and the model with the optimized assimilation of the Doppler currents (bottom). *(Source: Lewis et al., 1998.)*

radar systems to provide continuous year-long sea surface-current observations in a hostile environment where conventional instruments are unlikely to survive. A fairly wide area coverage (exceeding 500 km^2), high temporal resolution (entire surveillance area surveyed in a few minutes), immunity to weather conditions and suspended sediments, and land-based long-term monitoring are some of the key features of the Doppler radar systems. It is expected that these systems will play an important role in a wide variety of activities such as outfall design, effluent transport, pollution management, vessel traffic management in ports and harbors, and search and rescue of persons and crafts in distress as well as a host of other oceanographic and fisheries research programs. Doppler radar systems can gather a large amount of information. No other technique would enable such a comprehensive picture to be built up in a short period of time. The Doppler radar systems will definitely be of significant benefit to applied oceanography.

HF Doppler radar systems have begun to be a convenient tool for ocean current modelers as well. For example, Lewis et al. (1998) presented a technique for the assimilation of ocean surface currents determined from Doppler radar systems into numerical ocean models. They demonstrated an approach in which the Doppler radar current data act as though there were an additional layer of water overlying the ocean surface. A pseudo-shearing stress resulting from the difference between the model-predicted velocity in the Monterey Bay, California, region and the Doppler radar velocity was added to that of the wind in order to force a model. The numerical ocean model, with the optimized assimilation of the Doppler currents, provided a more realistic representation of the Monterey Bay currents relative to one without any assimilation of the Doppler currents (Figure 4.25).

4.12. ROUND-THE-CLOCK COAST- AND SHELF-OBSERVING ROLE OF DOPPLER RADAR

Many climatologists believe that in the coming decades, coastal oceans throughout the world are likely to undergo changes associated with climate change; increased levels of radioactive and other waste disposal into the seas; and increased levels of plumes, slicks, and so forth. Therefore, understanding the transport of sediment and the associated material from the harbor to the coastal ocean is a fundamental problem for water-quality managers. The plumes, which are usually dynamic in space and time, are modified by bottom topography, shoreline geometry, atmospheric forcing, tides, and river outflow. Fundamentally limiting our understanding of the seas around us is the inability to sample the ocean on relevant scales in both space and time. Our lack of understanding fuels the motivation to build regional integrated coastal ocean-observing networks. Such observing stations should be equipped to post the data to the Internet in real or near-real time through a series of Websites for distribution to people.

Coastally located land-based and offshore-located platform-mounted Doppler radars are well suited to indirectly examine several meteorological and environmental related activities happening on a large area of the sea surface through their capability for all-weather, round-the-clock monitoring of sea surface current and wave spectra distribution maps. Such a network would allow a person to sit at home during storms, tsunamis, oil slicks, or other oceanogenic hazards and monitor the sea surface motions in real time. This remote interaction is one of the hallmarks of coastal ocean-observing networks, and with several other parameters included in the observation scheme, it would be a transformational step for oceanographic research, material transport, routine environmental monitoring, search-and-rescue operations, and hazard mitigation efforts. For example, the New Jersey Shelf Observing System (NJSOS) uses hourly data from the sea surface current radar to indirectly monitor the Hudson River plume. Ocean color imagery and sea surface temperature from satellite-borne sensors provide maps that help define the spatial extent of this plume. These daily composites are then advected through time using the hourly data obtained from the radar. Through the combined application of the HF Doppler radar network and satellite imagery, environmental managers benefit from a real-time picture of the plume, allowing adaptive sampling and increased understanding of potential deposit centers of pollutants and other materials flowing out of the harbor (Schofield et al., 2005).

Continental shelf circulation is well known for its spatial variability. Until recently, the lack of data forced scientists, the U.S. Coast Guard, the U.S. Navy, and hazardous materials response groups to rely on the climatology of circulation patterns to conduct operations. Climatological approaches are not efficient enough in capturing the true variability of the circulation. Fortunately, an HF Doppler radar system, which is capable of remotely measuring sea surface currents as far offshore as 200 km, generates hourly maps indicating the speed and direction of the current at a number of spatially dense locations. These maps have great potential for search-and-rescue operations. Using the high-frequency Doppler radar network off the coast of New Jersey and near the mouth of Long Island Sound, demonstration projects have been conducted to provide proof of concept for using these surface current maps in Coast Guard search-and-rescue operations. Doppler radar data were found to be of immense practical use in defining the search areas. It was found that continuous spatial circulation data generated by the HF Doppler radar network allows a robust means to understand

advection of material on the continental shelf (thus benefiting science) while simultaneously providing the potential to greatly improve Coast Guard search-and-rescue operations (Schofield et al., 2005). Thus, HF Doppler radar networks, which are deployed and sustained on an operational basis, would serve as important ingredients for providing timely support for commercial and environmental communities. Many such networks are being deployed globally to complement other multisensor coastal-observing networks. Some are focused exclusively on research problems, but others have an applied focus. Success in the future will be measured by how the observatories simultaneously serve both of these needs.

4.13. DETECTION AND MONITORING OF TSUNAMI-INDUCED SEA SURFACE-CURRENT JETS AT CONTINENTAL SHELVES

When tsunami waves encounter steep gradients at the edges of continental shelves and at the coast, the waves become nonlinear, and conservation of momentum in the water column produces squirts (i.e., jets) of sea surface currents at areas of depth discontinuities and shallow regions. As discussed by Barrick (1979), a sinusoidal tsunami wave appears as a periodic surface current. Its wave orbital velocity at the surface transports the much shorter waves seen by the radar, adding to the ambient current field and producing a clear signature detectable by the radar. The tsunami, which is assumed to propagate perpendicular to the depth contours, produces sea surface current velocities that superimpose on the slowly varying ambient current velocity background. To some degree, there is an *a priori* pattern of large surface currents that occur when a tsunami encounters steep benthic gradients at the edge of a continental shelf. Tsunami currents have a characteristic signature due to their coherence over large distances, thereby allowing them to be detected when they arrive in the radar coverage area (Lipa et al., 2006).

Barrick (1979) originally proposed the use of shore-based HF radar systems for tsunami warning. HF radar systems currently operate continuously from many coastal locations around the globe, monitoring ocean surface currents and waves to distances of up to 200 km. For each HF radar location, it is possible to calculate a tsunami response pattern by numerical modeling methods (Lipa et al., 2006; Heron et al., 2008). To a first-order approximation, the response of the sea surface currents to the tsunami approaching the continental shelf is assumed to be independent of the direction of the source of the tsunami. This is because, as mentioned earlier, tsunami wave fronts are refracted in deep water and will approach the shelf edge within a small range of angles around orthogonal. This assumption can be tested for each site by numerical calculations provided by Greenslade et al. (2007). To simulate the signals seen by HF radar in case of a tsunami traveling toward the coast, Dzvonkovskaya et al. (2009) calculated the tsunami-induced sea surface current velocity using the oceanographic HAMburg Shelf Ocean Model (HAMSOM), then converted it into modulating signals and superposed to the measured radar backscatter signals. HAMSOM involves the friction and Coriolis terms and thus can simulate wave propagation from the deep ocean to shelf areas where nonlinear processes play an important role. After applying conventional signal processing techniques, the sea surface current maps contain the rapidly changing tsunami-induced current features, which can be compared to the HAMSOM data. The specific radial tsunami current signatures can clearly be observed in these maps, if appropriate spatial and temporal resolution is used. Gurgel et al. (2011) described a tsunami detection algorithm that can be used to issue an automated tsunami warning message. The sea surface current map based on these spectra has a pattern that changes very quickly in the shelf area before the tsunami wave reaches the beach. Specific radial tsunami current signatures are clearly observed in these maps. If the shelf edge is sufficiently far off the coast, the first appearance of such signatures can be monitored by an HF radar system early enough to issue a warning message about an approaching tsunami. The sea surface current response therefore becomes a signature that can be looked for in the data analysis process. Heron et al. (2008) have provided model calculations of sea surface current vectors when the first wave of the December 26, 2004, Indian Ocean tsunami encountered a section of the edge of the continental shelf of the Seychelles Island.

Lipa et al. (2006) demonstrated that HF Doppler radar systems in operation today are capable of detecting tsunami currents and providing vital information well before impact, when the adjacent continental shelf is wide. Heron et al. (2008) found that HF Doppler radar is well conditioned to observe the surface current bursts at the edge of the continental shelf and give a warning of 40 minutes to 2 hours when the shelf is 50 to 200 km wide. However, in the use of HF radar technology, there is a trade-off between the precision of surface current speed measurements and time resolution. An advantage in S/N ratio can be obtained from the prior knowledge of the spatial pattern of the squirts at the edge of the continental shelf. It was shown by Heron et al. (2008) that the phased array HF Doppler radar deployed in the Great Barrier Reef in Australia (where the shelf depth is about 50 m) and operating in a routine way for mapping sea surface currents can resolve surface current squirts from tsunamis in the wave period range 5−30 minutes and in the wavelength range greater than about 6 km. This network is found to be well conditioned for use as a monitor of small as well as larger tsunamis and

has the potential to contribute to the understanding of tsunami genesis.

When Doppler radar operates in its routine sea surface current-mapping mode, each station records a time-averaged (a few minutes) time series at a convenient sampling interval (say, 10 minutes). In this mode the radar could detect only tsunamis with wave periods greater than twice the sampling interval (Nyquist's sampling criterion). In other words, if the sampling interval is 10 minutes, the radar would detect only tsunamis with a wave period greater than 20 minutes. However, if the HF Doppler radar is to be used for detection of tsunami-induced magnified sea surface current jets (generated at depth discontinuities) for warning purposes, the radar would need to be switched to an "alert mode" of operation, presumably following a seismic alert. Lipa et al. (2006) suggested that in the event of a tsunami threat, tsunami watch software (producing current velocities and local wave information at the many HF radars in operation around the coastlines of the world) could run in parallel (in the background), activating a tsunami warning. This information would be available to local authorities and would be invaluable if international communications fail or are too general in their predictions. Global models may be inadequate for localized areas for which the available bathymetry may not be of adequate resolution. In addition, when a quake epicenter is close to shore, there may be insufficient time for the international communication chain to be activated. In such cases local systems would provide the only advance warning. Such a system may also alleviate the false-alarm problems that plague existing tsunami watch systems. Computer prediction models and early-warning schemes apply only to tsunamis generated by earthquakes; HF radar networks would also be able to detect tsunamis generated by underwater rockslides and tidal bores.

According to Heron et al. (2008), the most effective utility of an "alert mode" of operation would be in assisting the warning network by filling the gap between deep-ocean sensors and coastal sea-level gauges and, in particular, in avoiding false alarms because of its high sensitivity compared with other sensors. However, it is to be expected that a tsunami will be more difficult to detect if it is small or if the background current velocities due to tides, winds, or density gradients in the area monitored are large and rapidly varying. For the task of tsunami detection, the background current velocities can be considered a kind of "background noise" that needs to be removed to obtain the tsunami-induced currents more clearly.

The best way to handle this difficulty is to use an oceanographic model to simulate this "background noise." To keep the model result close to the actually measured ocean currents, it can be "guided" by applying a data assimilation technique (Gurgel et al., 2011). In a field application, a feasibility study would be required for each location, based on radar transmit frequency and taking into account the typical current regimes for the location, in addition to the bathymetry. It needs to be emphasized that if oceanographic radars are used for tsunami detection, they have to be operated in a high temporal (2 min) and spatial (1.5–2.0 km) resolution mode in order to have the best sensitivity and be able to resolve the quickly changing tsunami signatures. Gurgel et al. (2011) have found that a tsunami-induced sea surface current jet signature disappears completely at integration times larger than 25 min. They described a proposal for a new algorithm for automatic detection of tsunamis using a constant false alarm rate (CFAR) approach.

REFERENCES

Barrick, D., 1979. A coastal radar system for tsunami warning. Remote Sens. Environ. 8, 353–358.

Barrick, D.E., Headrick, J.M., Bogle, R.W., Crombie, D.D., 1974. Sea backscatter at HF: Interpretation and utilization of the echo. Proc. the Institute of Electrical & Electronic Engineers 62 (6), 673–680.

Barrick, D.E., Evans, M.W., Weber, B.L., 1977. Ocean surface currents mapped by radar. Science 198 (4313), 138–144.

Barrick, D.E., 1972. First-order theory and analysis of MH/HF/VHF scatter from the sea. IEEE Trans. Antennas Propagation AP-20, 2–10.

Barrick, D.E., 1980. Accuracy of parameter extraction from sample averaged sea echo Doppler spectra. IEEE Trans. Antennas Propagation 28, 1–11.

Barrick, D.E., 1986. The role of the gravity-wave dispersion relation in HF radar measurements of the sea surface. IEEE J. Ocean. Eng. OE-11 (2), 286–292.

Barrick, D.E., Lipa, B.J., 1986. Correcting for distorted antenna patterns in CODAR ocean surface measurements. IEEE J. Ocean. Eng. OE-11 (2), 304–309.

Barrick, D.E., Lipa, B.J., Crissman, R.D., 1985. Mapping surface currents with CODAR. Sea Technol. 26, 43–48.

Broche, P., Crochet, J.C., de Maistre, J.L., Forget, P., 1987. VHF radar for ocean surface current and sea state remote sensing. Radio Sci. 22, 69–75.

Broche, P., Crochet, J.C., de Maistre, J.C., Forget, P., 1987. VHF radar for ocean surface current and sea state remote sensing. Radio Sci. 22, 69–75.

Chapman, R.D., Shay, L.K., Graber, H.C., Edson, J.B., Karachintsev, A., Trump, C.L., Ross, D.B., 1997. On the accuracy of HF radar surface current measurements: Intercomparison with ship-based sensors. J. Geophys. Res. 102 (C8), 18,737–18,748.

Cochin, V., Mariette, V., Broche, P., Garello, R., 2006. Tidal current measurements using VHF radar and ADCP in the Normand Breton Gulf: Comparison of observations and numerical model. IEEE J. Ocean. Eng. 31 (4), 885–893.

Collar, P.G., 1993. A review of observational techniques and instruments for current measurements from the open sea. Report No. 304, Institute of Oceanographic Sciences, Deacon Laboratory, Brook road, Wormley, Godalming, Surrey, UK.

Collar, P.G., Howarth, M.J., 1987. A comparison of three methods of measuring surface currents in the sea: Radar, current meters and

surface drifters. Department of Energy Offshore Technology Report No. OTH 87272.

Crombie, D.D., 1955. Doppler spectrum of sea echo at 13.56 Mc/s. Nature 175 (4459), 681–682.

Crombie, D.D., 1972. Resonant backscatter from the sea and its application to physical oceanography. Proc. IEEE Oceans '72 Conference, 172–179.

Dzvonkovskaya, A., Gurgel, K.W., Pohlmann, T., Schlick, T., Xu, J., 2009. Simulation of tsunami signatures in ocean surface current maps measured by HF radar. Proc. IEEE.

Eccles, D., 1989. The Ocean Surface Current Radars. Rutherford Appleton Laboratory Report.

Emery, B.M., Washburn, L., Harlan, J.A., 2004. Evaluating radial current measurements from CODAR high-frequency radars with moored current meters. J. Atmos. Oceanic Technol. 21, 1259–1271.

Essen, H.H., Gurgel, K.W., Schirmer, F., 1983. Tidal and wind-driven parts of surface currents as measured by radar. Dt. Hydrogr. Z 36, 81–96.

Frisch, A.S., Weber, B.L., 1980. A new technique for measuring tidal currents by using a two-site HF Doppler radar system. J. Geophys. Res. 85, 485–493.

Georges, T.M., 1981. Measuring ocean currents with HF radar. Proc. Oceans '81 IEEE Conference record 1, 228–232.

Georges, T.M., Harlan, J.A., 1995. Mapping surface currents near the Gulf Stream using the Air Force over-the-horizon radar. Proc. IEEE Fifth Working Conference on Current Measurements, 115–120.

Graber, H.C., Haus, B.K., Chapman, R.D., Shay, L.K., 1997a. HF radar comparisons with moored estimates of current speed and direction: Expected differences and implications. J. Geophys. Res. 102, 18,749–18,766.

Greenslade, D.J.M., Simanjuntak, M.A., Burbidge, D., Chittleborough, J., 2007. A first-generation real-time tsunami forecasting system for the Australian Region. BMRC Report No. 126. Bureau of Meteorology, Australia.

Gurgel, K.W., Dzvonkovskaya, A., Pohlmann, T., Schlick, T., Gill, E., 2011. Simulation and detection of tsunami signatures in ocean surface currents measured by HF radar. Ocean Dynamics.

Gurgel, K.W., Antonischki, G., Schlick, T., 1997. A comparison of surface current fields derived by beam-forming and direction-finding techniques as applied to the HF radar WERA. IGARSS Proceedings Singapore.

Gurgel, K.W., Antonischki, G., Schlick, T., 1997. A comparison of surface current fields derived by beam-forming and direction-finding techniques as applied to the HF radar WERA. IGARSS Proceedings.

Gurgel, K.W., Antonischki, G., Essen, H.H., Schlick, T., 1999b. Wellen Radar (WERA): A new ground-wave HF radar for ocean remote sensing. Coastal Engineering 37, 219–234.

Gurgel, K.W., Antonishki, G., Essen, H.H., Schlick, T., 1999a. Wellen Radar (WERA), a new ground-wave based HF radar for ocean remote sensing. Coast. Eng. 37, 219–234.

Gurgel, K.W., Essen, H.H., Schirmer, F., 1986. CODAR in Germany: A status report valid November 1985. IEEE Journal of Oceanic Engineering OE-11 (2), 251–257.

Gurgel, K.W., Essen, H.-H., Kingsley, S.P., 1999a. High-frequency radars: physical limitations and recent developments. Coastal Engineering 37, 201–218.

Ha, E.C., 1979. Remote sensing of ocean surface current and current shear by HF backscatter radar. Ph.D. dissertation. Stanford University, Stanford, CA, USA.

Hammond, T.M., Pattiaratchi, C.B., Eccles, D., Osborne, M.J., Nash, L.A., Collins, M.B., 1987. Ocean surface current radar (OSCR) vector measurements on the inner continental shelf. Contin. Shelf Res. 7, 411–431.

Heron, M.L., Prytz, A., Heron, S.F., Helzel, T., Schlick, T., Greenslade, D.J.M., Schulz, E., Skirving, W.J., 2008. Tsunami observations by coastal ocean radar. International Journal of Remote sensing 29 (21), 6347–6359.

Heron, M.L., Dexter, P.E., McGann, B.T., 1985. Parameters of the air–sea interface by high-frequency ground-wave HF Doppler radar. Aust. J. Mar. Freshwater Res. 36, 655–670.

Hickey, K., Khan, R.H., Walsh, J., 1995. Parametric estimation of ocean surface currents with HF radar. IEEE J. Oceanic Eng. 20, 139–144.

Hill, D.A., Wait, J.R., 1980. Ground-wave attenuation function for a spherical earth with arbitrary surface impedance. Radio Sci. 15, 637–643.

Holbrook, J.R., Frisch, A.S., 1981. A comparison of near-surface CODAR and VACM measurements in the Strait of Juan de Fuca, August 1978. J. Geophys. Res. 86, 10,908–10,912.

Janopaul, M.M., Broche, P., De Maistre, J.C., Essen, H.H., Blanchet, C., Grau, G., Mittelstaedt, E., 1982. Comparison of measurements of sea currents by HF radar and by conventional means. International Journal of Remote Sensing 3, 409–422.

Jeans, P.K., Donnelly, R., 1986. Four-element CODAR beam forming. IEEE J. Oceanic Eng. OE-11 (2), 296–303.

Kim, S.Y., Terrill, E., Cornuelle, B., 2007. Objectively mapping HF radar-derived surface current data using measured and idealized data covariance matrices. J. Geophys. Res. 112 (C06021), 1–16.

Kohut, J., Glenn, S., Barrick, D., 1999. SeaSonde is integral to coastal flow model development. Hydro Int. 3, 32–35.

Lane, A., Knight, P.J., Player, R.J., 1999. Current measurement technology for near-shore waters. Coastal Engineering 37, 343–368.

Leise, J.A., 1984. The analysis and digital signal processing of NOAA's surface current mapping system. IEEE Journal of Oceanic Engineering OE-9 (2), 106–113.

Lewis, J.K., Shulman, I., Blumberg, A.F., 1998. Assimilation of Doppler radar current data into numerical ocean models. Cont. Shelf Res. 18, 541–559.

Lillesand, T.M., Kiefer, R.W., 1979. Remote sensing and image interpretation, second ed. Wiley.

Lipa, B., 2003. HF radar current velocity uncertainties. Sea Technol. 44 (9), 81–81.

Lipa, B.J., Barrick, D.E., 1983. Least-squares methods for the extraction of surface currents from CODAR crossed-loop data: Application at ARSLOE. IEEE J. Ocean. Eng. OE-8 (4), 226–253.

Lipa, B.J., Barrick, D.E., Bourg, J., Nyden, B.B., 2006. HF Radar detection of tsunamis. Journal of Oceanography 62, 705–716.

Lipa, B., Nyden, B., Ullman, D.S., Terrill, E., 2006. SeaSonde radial velocities: Derivation and internal consistency. IEEE J. Oceanic. Eng. 31 (4), 850–861.

Mantovanelli, A., Heron, M.L., Prytz, A., 2010. The use of HF radar surface currents for computing Lagrangian trajectories: Benefits and issues. IEEE 2010, Washington, DC, U.S.A.

Maresca Jr., J., Carlson, C., 1980. Comment on "Longshore currents on the fringe of hurricane Anita, " by N. P. Smith. J. Geophys. Res. 85 (C3), 1640–1641.

Matthews, J.P., Simpson, J.H., Brown, J., 1988. Remote sensing of shelf sea currents using a high-frequency ocean surface current radar system. J. Geophys. Res. 93 (C3), 2303–2310.

Ohlmann, C., White, P., Washburn, L., Terrill, E., Emery, B., Otero, M., 2007. Interpretation of coastal HF Radar derived surface currents with high-resolution drifter data. J. Atmos. Oceanic Technol. 24, 666–680.

Ohlmann, J.C., White, P.F., Sybrandy, A.L., Niller, P.P., 2005. GPS-cellular drifter technology for coastal ocean observing systems. J. Atmos. Oceanic Technol. 22, 1381–1388.

Paduan, J.D., Shulman, I., 2004. HF radar data assimilation in the Monterey Bay area. J. Geophys. Res. 109 (C07 S09), 1–17.

Paduan, J.D., Rosenfeld, L.K., 1996. Remotely sensed surface currents in Monterey Bay from shore-based HF radar (Coastal Ocean Dynamics Application Radar). J. Geophys. Res. 101, 20,669–20,686.

Paduan, J.D., Barrick, D., Fernandez, D., Hallock, Z., Teague, C., 2001. Improving the accuracy of coastal HF radar current mapping. Hydro Int. 5, 26–29.

Paduan, J.D., Petruncio, E.T., Barrick, D.E., Lipa, B.J., 1995. Surface currents within and offshore of Monterey Bay as mapped by a multiple-site HF radar (CODAR) network. Proc. 1EEE Fifth Working Conference on Current Measurements, 137–142.

Pandian, P.K., Emmanuel, O., Ruscoe, J.P., Side, J.C., Harris, R.E., Kerr, S.A., Bullen, C.R., 2010. An overview of recent technologies on wave and current measurement in coastal and marine applications. Journal of Oceanography and Marine Sciences 1 (1), 1–10.

Parker, K., 1989. Surface current radar: Boon to coastal engineers. Sea Technol. 30 (2), 60–65.

Ponsford, T., Srivastava, S., 1990. Groundwave over-the-horizon radar development at NORDCO. NORDCO Limited.

Prandle, D., 1987. The fine structure of near-shore tidal and residual circulations revealed by HF radar surface current measurements. J. Phys. Oceanogr. 17, 231–245.

Prandle, D., Ryder, D.K., 1985. Measurements of surface currents in Liverpool Bay by high-frequency radar. Nature 315, 128–131.

Prandle, D., Loch, S.G., Player, R., 1992. Tidal flow through the straits of Dover. J. Phys. Oceanogr. 23, 23–37.

Schmidt, R.O., 1986. Multiple emitter location and signal parameter estimation. IEEE Trans. Antennas Propag. AP-34 (3), 276–280.

Schofield, O., Kohut, J., Glenn, S., 2005. The New Jersey shelf observing system. Sea Technol. 46 (9), 15–21.

Schott, F.A., Frisch, S.A., Larsen, J.C., 1986. Comparison of surface currents measured by HF Doppler Radar in the Western Florida straits during November 1983 to January 1984 and Florida current transports. J. Geophys. Res. 91 (C7), 8451–8460.

Shay, L.K., Graber, H.C., Ross, D.B., Chapman, R.D., 1995. Mesoscale ocean surface current structure detected by high-frequency radar. J. Atmos. Ocean. Technol. 12, 881–900.

Shay, L.K., Graber, H.C., Ross, D.B., Chapman, R.D., 1995. Mesoscale ocean surface current structure detected by high-frequency radar. J. Atmos. Oceanic Technol. 12, 881–900.

Shay, L.K., Lentz, S.J., Graber, H.C., Haus, B.K., 1998. Current structure variations detected by high-frequency radar and vector-measuring current meters. J. Atmos. Oceanic Technol. 15, 237–256.

Shearman, E.D.R., 1986. A review of methods of remote sensing of sea-surface conditions by HF radar and design considerations for narrow-beam systems. IEEE J. Ocean. Eng. OE-11 (2), 150–157.

Shearman, E.D.R., Moorhead, M.D., 1988. PISCES: A coastal groundwave HF radar for current, wind, and wave mapping to 200-km ranges. Proceedings IGARSS '88, 773–776.

Skop, R.A., Graber, H.C., Ross, D.B., 1995. VHF radar measurements of flow patterns in bays and estuaries. Proc. IEEE Fifth Working Conference on Current Measurements, 143–147.

Stewart, R.H., Joy, J.W., 1974. HF radio measurements of surface currents. Deep-Sea Res. 21, 1039–1049.

Takeoka, H., Tanaka, Y., Ohno, Y., Hisaki, Y., Nadai, A., Kuroiwa, H., 1995. Observation of the Kyucho in the Bungo Channel by HF radar. J. Oceanogr. 51, 699–711.

Teague, C.C., 1986. Multifrequency HF radar observations of currents and current shears. IEEE Journal of Oceanic Engineering OE-11 (2), 258–269.

Vigan, X., 2002. Upper-layer ocean current forecasts. Sea Technol. 43 (10), 15–19.

Wait, J.R., 1966. Theory of HF ground wave backscatter from sea waves. J. Geophys. Res. 71 (20), 4839–4842.

Weber, B.L., Barrick, D.E., 1977. On the nonlinear theory for gravity waves on the ocean's surface, Part I: Derivations. Journal of Physical Oceanography 7, 3–10.

Wu, J., 1975. Sea surface drift-currents. Proc. Offshore Technology Conference 2, 477–484.

Wyatt, L.C., Thompson, S.P., Burton, R.R., 1999. Evaluation of HF radar wave measurements. Coastal Engineering 37, 259–282.

BIBLIOGRAPHY

Abascal, A.J., Castanedo, S., Medina, R., Losada, I.J., Fanjul, E.A., 2009. Application of HF radar currents to oil spill modeling. Mar. Poll. Bull. 58, 238–248.

AHQ Survey Coy, 1942. AHQ Survey Coy by Authority of Director of Survey, 1942.

Anderson, S., 2011. HF skywave radar performance in the tsunami detection and measurement role. In: Czerwinski, F. (Ed.), InTechOpen (Open Access to Knowledge). The tsunami threat: Research and technology Chapter 31, pp. 641–666.

Backhaus, J.O., 1985. A three-dimensional model for the simulation of shelf sea dynamics. Dt. Hydrogr. Z. 38, 165–187.

Barrick, D., 2003. Proliferation of SeaSonde coastal current-mapping radars. Hydro Int. 7 (1), 30–33.

Barrick, D.E., 1971. Theory of HF and VHF propagation across the rough sea: 2. Application to HF and VHF propagation above the sea. Radio Sci 6, 527–533.

Barrick, D.E., 1977. Extraction of wave parameters from measured HF radar sea-echo Doppler spectra. Radio Science 12, 415–424.

Barrick, D.E., 1978. H. F. radio oceanography: A review. Bound Layer Meteor 13, 23–43.

Barrick, D.E., 1998. Grazing behaviour of scatter and propagation above any rough surface, IEEE Trans. Antennas. Propag. 46, 73–83.

Barrick, D.E., Lipa, B.J., 1996. Comparison of direction-finding and beam-forming in HF Radar Ocean surface current mapping. Phase 1 SBIR Final Report. Contract No. 50-DKNA-5-00092. NOAA, Rockville, MD, USA.

Barrick, D.E., Lipa, B.J., 1997. Evolution of bearing determination in HF current mapping radars. Oceanography 10, 72–75.

Barrick, D.E., Lipa, B.J., 1986. Correcting for distorted antenna patterns in CODAR ocean surface measurements. IEEE J. Ocean. Engr. OE-11, 304–309.

Barrick, D.E., Snyder, J.A., 1977. The statistics of HF sea-echo Doppler spectra. IEEE Trans. Antennas Propag. AP-25 (1), 19−28.

Bendat, J.S., Piersol, A.G., 2000. Random data analysis and measurement procedures. Wiley Interscience.

Bilham, R., Engdahl, R., Feldl, N., Satyabala, S.P., 2005. Partial and complete rupture of the Indo-Andaman plate boundary, 1847−2004. Seismol. Res. Lett. 76 (3), 299−311.

Bjorkstedt, E., Roughgarden, J., 1997. Larval transport and coastal upwelling: An application of HF radar in ecological research. Oceanography 10, 64−67.

Broche, P., Salomon, J.P., Demaistre, J.S., Devenon, J.L., 1986. Tidal currents in Baie de Seine: Comparison of numerical modeling and high-frequency radar measurements. Estuarine Coastal Shelf Sci. 23, 465−476.

Bryant, E., 2001. Tsunami: The underrated hazard. Cambridge University Press, Cambridge, UK.

Collar, P.G., Howarth, M.J., 1987. A comparison of three methods of measuring currents in the sea: RADAR, current meters and surface drifters. Department of Energy, Offshore Technology Report, OTH 87 272 London, HMSO.

Collar, P.G., Howarth, J.M., Millard, N.W., Eccles, D., 1985. An intercomparison of HF radar observations of surface currents with moored current meter data and displacement rates of acoustically tracked drogued floats: Evaluation, comparison and calibration of oceanographic instruments, Proceedings of an international conference. Advances in Underwater Technology and Offshore Engineering. Graham & Trotman, 163−182.

Dankert, H., Rosenthal, W., 2004. Ocean surface determination from X-band radar-image sequences. J. Geophys. Res. 109, C04016.

Dzvonkovskaya, A., Gurgel, K.W., Rohling, H., Schlick, T., 2008. Low power, high frequency surface wave radar application for ship detection and tracking. Proc. Radar 2008 Conf. Adelaide, Australia, 654−659.

Dzvonkovskaya, A., Gurgel, K.W., Pohlmann, T., Schlick, T., Xu, J., 2009a. Simulation of tsunami signatures in ocean surface current maps measured by HF radar. Proc. Oceans 2009 Conf. Bremen, Germany.

Dzvonkovskaya, A., Gurgel, K.W., Pohlmann, T., Schlick, T., Xu, J., 2009b. Tsunami detection using HF radar WERA: A simulation approach. Proc. Radar 2009 Conf. Bordeaux, France.

Essen, H.H., Gurgel, K.W., Schlick, T., 2000. On the accuracy of current measurements by means of HF radar. IEEE J. Oceanic. Eng. 25 (4), 472−480.

Essen, H.H., Gurgel, K.W., Schirmer, F., Sirkes, Z., 1995. Horizontal variability of surface currents in the Dead Sea. Oceanol. Acta. 18, 455−467.

Essen, H.-H., Gurgel, K.W., Schirmer, F., 1983. Tidal and wind-driven parts of surface currents as measured by radar. Dtsch. Hydrogr. Z. 36, 81−96.

Essen, H.-H., Gurgel, K.W., Schirmer, F., 1989. Surface currents in the Norwegian Channel measured by radar in March 1985. Tellus 41A, 162−174.

Fernandez, D.M., Graber, H.C., Paduan, J.D., Barrick, D.E., 1997. Mapping wind direction with HF radar. Oceanography 10, 93−95.

Fernandez, D.M., Vesecky, J.F., Teague, C.C., 1995. Measurement of upper-ocean surface currents with high-frequency radar. Proc. IEEE Fifth Working Conference on Current Measurements, 109−114.

Frisch, A.S., Weber, B.L., 1980. A new technique for measuring tidal currents by using a two-site HF Doppler Radar System. J. Geophys. Res. 85 (C1), 485−493.

Frisch, A.S., Weber, B.L., 1982. Application of dual-Doppler HF radar measurements of ocean surface currents. Remote Sensing of Environment 12, 273−282.

Gill, E.W., Walsh, J., 2001. High-frequency bistatic cross-sections of the ocean surface. Radio Sci. 36 (6), 1459−1475.

Gill, E.W., 1999. The scattering of high frequency electromagnetic radiation from the ocean surface: An analysis based on bistatic ground wave radar configuration. Ph.D. thesis. Memorial University of Newfoundland, St. John's, Canada.

Gonella, J., 1972. A rotary-component method for analysing meteorological and oceanographic vector time series. Deep-Sea Res. 19, 833−846.

Gower, J., 2005. Jason 1 detects the 26 December 2004 tsunami. American Geophysical Union EOS 86, 37−38.

Graber, H.C., Limouzy-Paris, C.B., 1997b. Transport patterns of tropical reef fish larvae by spin-off eddies in the Straits of Florida. Oceanography 10, 68−71.

Griffiths, C.R., MacDougall, N., 1998. The Tiree Passage mooring 1981−1997. Dunstaffnage Marine Laboratory, Marine Technology Report No. 145.

Gurgel, K.W., 1994. Shipborne measurement of surface current fields by HF radar. L'Onde Electrique 74, 54−59.

Gurgel, K.W., 1997. Experience with ship-borne measurements of surface current fields by radar. Oceanography 10, 82−84.

Gurgel, K.W., Barbin, Y., Schlick, T., 2007. Radio frequency interference suppression techniques in FMCW modulated HF radars. Proc. IEEE/OES Oceans 2007 Europe, Aberdeen, Scotland, UK.

Hasselmann, K., 1971. Determination of ocean wave spectra from Doppler radio return from the sea surface. Nature Physical Science 229, 16−17.

Heron, M.L., Prytz, A., Heron, S.F., Helzel, T., Schlick, T., Greenslade, D.J.M., Schulz, E., Skirving, W.J., 2008. Tsunami observations by coastal ocean radar. Int. J. Remote Sens. 29 (21), 6347−6359.

Hodgins, D.O., 1994. Remote sensing of ocean surface currents with the SeaSonde HF radar. Spill Sci. Technol. Bull. 1, 109−129.

Holbrook, J.R., Frisch, A.S., 1981. A Comparison of near-surface CODAR and CACAM measurements in the Strait of Juan De Fuca, August 1978. J. Geophys. Res. 86 (C11), 10,908−10,912.

Howarth, M.J., Harrison, A.J., Knight, P.J., Player, R.J., 1995. Measurement of net flow through a channel. IEEE Fifth Working Conference on Current Measurement, 121−126.

Janopaul, M.M., Broche, P., de Maistre, J.C., Essen, H.H., Blanchet, C., Grau, G., Mittelstaedt, E., 1982. Comparison of measurements of sea currents by HF radar and by conventional means. Int. J. Remote Sens. 3, 409−422.

Kaplan, D.M., Largier, J., Botsford, L.W., 2005. HF radar observations of surface circulation off Bodega Bay (northern California, USA). J. Geophys. Res. 110, C10020.

Khan, R.H., 1991. Ocean-clutter model for high-frequency radar. IEEE J. Oceanic Eng. 16, 181−188.

King, J.W., co-authors, 1984. OSCR (Ocean Surface Current Radar) observations of currents off the coasts of Northern Ireland, England, Wales and Scotland, Current measurements off shore. Soc. Underwater Technol.. London, UK.

Kinsman, B., 1965. Wind waves. Prentice-Hall, Englewood Cliffs, NJ, USA.

Klinck, J.M., 1985. EOF analysis of central Drake Passage currents from DRAKE 79. J. Phys. Oceanogr. 15, 288−298.

Knight, P.J., Howarth, M.J., 1998. The flow through the North Channel of the Irish Sea. Continental Shelf Res. 19, 693–716.

Kohut, J.T., Glenn, S.M., 2003. Improving HF radar surface current measurements with measured antenna beam patterns. J. Atmos. Oceanic Technol. 20, 1303–1316.

Kosro, P.M., Barth, J.A., Strub, T.P., 1997. The coastal jet: Observations of surface currents over the Oregon continental shelf from HF radar. Oceanography 10 (2), 53–57.

Laws, K.E., Fernandez, D.M., Paduan, J.D., 2000. Simulation-based evaluations of HF radar ocean current algorithms. IEEE J. Oceanic Eng. 25, 481–491.

Ledgard, L.J., Webster, S., Wyatt, L.R., 1996. The measurement of ocean waves along the Holderness Coast using OSCR. UK Oceanography '96 Programme and abstracts, IEEE Conference publication.

Leise, J.A., 1981. The analysis and digital signal processing of NOAA's surface current mapping radar. IEEE J. Oceanic Eng. 9, 106–113.

Leise, J.A., 1984. The analysis and digital signal processing of NOAA's surface current mapping system. IEEE J. Oceanic Eng. OE-9, 106–113.

Lipa, B.J., Barrick, D.E., 1983. Least-squares methods for the extraction of surface currents from CODAR crossed-loop data: Application at ARSLOE. IEEE J. Ocean. Eng. OE-8 (4), 226–253.

Lipa, B., Barrick, D., Bourg, J., Nyden, B., 2006b. HF radar detection of tsunami. J. Oceanogr. 62, 705–716.

Lyzenga, D., Nwogu, O., Trizna, D., 2009. Ocean wave field measurements using coherent and non-coherent radars at low grazing angles. IGARSS 2010. Honolulu, HI, USA, 26–30.

Martin, R.-J., Kearney, M.J., 1997. Remote sea current sensing using HF radar: An autoregressive approach. IEEE J. Oceanic Eng. 22, 151–155.

Matthews, J.P., Fox, A.D., Prandle, D., 1993. Radar observation of an along-front jet and transverse flow convergence associated with a North Sea front. Continental Shelf Res. 13, 109–130.

Melton, D.C., 1995. Remote sensing and validation of surface currents from HF radar. M.S. thesis. Naval Postgraduate School.

Orr, W.I., 1978. Radio Handbook, twentyfirst ed. Editors and Engineers, Indianapolis, IN, USA.

Osborne, M.J., 1991. OSCR and Interocean S4 current measurements in Poole Bay. Underwater Technology 17, 10–18.

Paduan, J.D., Graber, H.C., 1997. Introduction to high frequency radar: Reality and myth. Oceanography 10, 36–39.

Paduan, J.D., Kim, K.C., Cook, M.S., Chavez, F.P., 2006. Calibration and validation of high-frequency radar ocean surface current observations. IEEE J. Ocean. Eng. 31 (4), 862–875.

Peters, N.J., Skop, R.A., 1997. Measurements of ocean surface currents from a moving ship using VHF radar. J. Atmos. Oceanic Technol. 14, 676–694.

Pierson, W., Moskowitz, L., 1964. A proposed spectral form for fully developed seas based upon the similarity theory of S.A. Kitaigorodskii. J Geophys. Res. 69 (24), 5181–5190.

Player, R.J., Radar, H.F., 1995. (OSCR) surface current measurements in the North Channel. July 1993–August 1994, Proudman Oceanographic Laboratory, Joseph Proudman Building, 6 Brownlow street, Liverpool LB 5DA, United Kingdom. Report No. 40.

Prandle, D., 1985b. Measuring Currents at the sea surface by H.F. Radar (OSCR). J. Soc. Underwater Technol. 11 (2), 25–27.

Prandle, D., 1987. The fine structure of near-shore tidal and residual circulations revealed by HF radar surface current measurements. J. Phys. Oceanography 17, 231–245.

Prandle, D., 1991. A new view of near-shore dynamics based on observations from H.F. radar. Progress in Oceanography 27, 403–438.

Prandle, D., Ryder, D.K., 1985. Measurement of surface current in Liverpool Bay by high-frequency radar. Nature 315 (6015), 128–131.

Prandle, D., Howarth, J., 1986. The use of HF radar measurements of surface currents for coastal engineers. In: Int. Conf. on Measuring Techniques of Hydraulics Phenomena in Offshore Coastal and Inland Waters. London, BHRA, Cranfield, UK.

Richman, J.G., de Szoeke, R.A., Davis, R.E., 1987. Measurements of near-surface shear in the ocean. J. Geophys. Res. 92 (C3), 2851–2858.

Rohling, H., 1983. Radar CFAR thresholding in clutter and multiple target situations. IEEE Trans. Aerosp. Electron. Syst. AES 19, 608–621.

Shearman, E.D.R., 1983. Propagation and scattering in mf/hf groundwave radar. IEEE Proc. (F) 130, 579–590.

Sixt, M., Parent, J., Bourdillon, A., Delloue, J., 1996. A new multibeam receiving equipment for the Valensole Skywave HF radar: description and applications. IEEE Trans. Geosci. Remote Sens. 34, 708–719.

Smith, W.H.F., Scharroo, R., Titov, V.V., Arcas, D., Arbic, B.K., 2005. Satellite altimeters measure tsunami. Oceanography 18, 11–13.

Stewart, R.H., Joy, J.W., 1974. H.F. radio measurements of surface currents. Deep-Sea Res. 21, 1039–1049.

Trizna, D.B., 2001. Errors in bathymetric retrievals using linear dispersion in 3D FFT analysis of marine radar ocean wave imagery. IEEE Trans. Geosciences and Remote Sensing 39, 2465–2469.

Trizna, D.B., 2009. A coherent marine radar for decameter-scale current mapping and direct measurements of directional ocean wave spectra. OCEANS 2009. Biloxi MS, USA, 1–6.

Trizna, D.B., 2010. Coherent marine radar measurements of properties of ocean waves and currents. Proceedings of IGARSS 2010. Honolulu, HI, USA, 23–27.

U.S. Government Accounting Office, 2010. U.S. tsunami preparedness. GAO Report 10–490, April 2010.

Ullman, D.S., O'Donnell, J., Kohut, J., Fake, T., Allen, A., 2006. Trajectory prediction using HF radar surface currents: Monte Carlo simulations of prediction uncertainties. J. Geophys. Res. 111, C12005.

Wait, J.R., 1962. Electromagnetic waves in stratified media. Pergamon Press, New York, NY, USA.

Wyatt, L.R., Ledgard, L.J., 1996. OSCR Wave Measurements—some preliminary results. IEEE J. Oceanic Eng. 21 (1), 64–76.

Yoshikawa, Y., Masuda, A., Marubayashi, K., Ishibashi, M., Okuno, A., 2006. On the accuracy of HF radar measurement in the Tsushima Strait. J. Geophys. Res. 111 (C04009), 1–10.

Young, I.R., Rosenthal, W., Ziemer, F., 1985. A three-dimensional analysis of marine radar images for the determination of ocean wave directionality and surface currents. J. Geophys. Res. 90, 1049–1059.